




Amplification and ellipticity enhancement of high-order harmonics in a neonlike x-ray laser dressed by an IR field

V. A. Antonov ^{1,*} I. R. Khairulin ¹ M. Yu. Ryabikin ^{1,2} M. A. Berrill,³
V. N. Shlyaptsev,³ J. J. Rocca,^{3,4} and Olga Kocharovskaya⁵

¹*Institute of Applied Physics of the Russian Academy of Sciences, 46 Ulyanov Street, Nizhny Novgorod 603950, Russia*

²*Lobachevsky State University of Nizhny Novgorod, 23 Prospekt Gagarina, Nizhny Novgorod 603950, Russia*

³*Department of Electrical and Computer Engineering, Colorado State University, Fort Collins, Colorado 80523, USA*

⁴*Department of Physics, Colorado State University, Fort Collins, Colorado 80523, USA*

⁵*Department of Physics and Astronomy and Institute for Quantum Science and Engineering, Texas A&M University, 578 University Drive, College Station, Texas 77843-4242, USA*



(Received 17 April 2021; revised 23 February 2023; accepted 2 May 2023; published 20 June 2023)

In Khairulin *et al.* [*Sci. Rep.* **12**, 6204 (2022)] we proposed a method for amplifying a train of sub-femtosecond pulses of circularly or elliptically polarized extreme ultraviolet radiation, composed by high-order harmonics of an infrared (IR) laser field, in a neonlike active medium of a plasma-based x-ray laser, additionally irradiated with a replica of a fundamental frequency laser field used to generate harmonics. Here we present the analytical theory and numerical study of an amplification process of an individual harmonic with either preservation of its polarization state or ellipticity enhancement. We also analyze in detail the spectral-temporal and polarization properties of a sub-femtosecond pulse train formed by a set of elliptically or circularly polarized harmonics during the propagation through the medium. We discuss also the possibility of an experimental implementation of the suggested technique in an active medium of an x-ray laser based on neonlike Ti^{12+} ions irradiated by an IR laser field with a wavelength of 3.2 μm .

DOI: [10.1103/PhysRevA.107.063511](https://doi.org/10.1103/PhysRevA.107.063511)

I. INTRODUCTION

Sub-femtosecond (sub-fs) pulses of extreme ultraviolet (XUV) and x-ray radiation produced via high-harmonic generation (HHG) of optical laser fields have enabled for the first time an experimental study of ultrafast electronic processes in atoms, molecules, and solids on their intrinsic timescales [1–4]. However, typically such pulses are linearly polarized, which prevents one from using them for the investigation of chiral and magnetic media. Generation of bright elliptically and circularly polarized high-order harmonics (HHs) of optical radiation is a difficult task for various reasons.

First, the harmonic generation efficiency decreases rapidly with increasing ellipticity of the fundamental laser field [5,6], because, in accordance with the semiclassical model of HHG [7], when the polarization of the electric field differs from linear, the freed electrons move along curved paths; in this case, the electron trajectories, which at the moment of release from the atom had a transverse velocity close to zero, subsequently miss the parent ion. The analysis shows that, typically, the longer the electron trajectory, the lower the ellipticity of the produced harmonics, which is due to the spreading of the electron wave packet [8]. The exceptions are the cases of harmonic frequencies satisfying the conditions of a resonance below the ionization threshold or continuum resonance of the

target. For both cases, the resonant HHG enhancement has been observed in [9], where the interactions of elliptically polarized laser field with Ar atoms and SF_6 molecules resulted in enhanced elliptically polarized harmonic production due to, respectively, resonances below and above the ionization threshold I_p . The maximum ellipticity of resonantly enhanced harmonics in both cases reached 0.75–0.8. It should be noted, however, that such a resonant enhancement was observed only in a narrow interval of harmonic photon energies near 15.3 eV (Ar) and in the range 20–27 eV (SF_6).

One of the alternative approaches to producing elliptically or circularly polarized HHs involves the generation of linearly polarized harmonics upon irradiation of gases by a linearly polarized laser field, with further conversion of the generated radiation into elliptically polarized using phase-shifting optics. For example, the use of phase retarders based on a sequence of mirrors [10] and multilayer quarter waveplates [11] was demonstrated experimentally. Among the drawbacks of the demonstrated schemes of this kind are their low (about few percent) transmission efficiency and narrow frequency tuning region (not exceeding several eV).

A number of experimental studies have demonstrated methods for producing an elliptically polarized XUV radiation directly in the HHG process. One of the proposed approaches consists in generating elliptically polarized harmonics in a gas of aligned molecules. However, in the linearly polarized laser field the harmonic ellipticity in this case did not exceed 0.4 [12], while HHG by circularly polarized laser field was quite inefficient [13].

*antonov@appl.sci-nnov.ru

Much attention has been paid to HHG schemes using multicomponent laser fields, whose components have different carrier frequencies and intensities, as well as, in the general case, polarizations. For example, recent experiments [14,15] demonstrated the generation of harmonics with ellipticity reaching 0.7–0.75 in noble gases exposed to a two-component laser field, which is a superposition of fundamental-frequency and second-harmonic fields with mutually orthogonal linear polarizations. It turns out, however, that in the case of low-intensity second-harmonic field [14], high ellipticity is achieved only for even-order harmonics, whose intensity is low. In the case when the intensity of the second-harmonic field was scanned [15], the even- and odd-order harmonics of comparable intensity were obtained. However, it turns out that in this scheme the harmonics radiated from two adjacent half optical cycles have opposite helicity; moreover, the even- and odd-order harmonics have different polarization directions. Thus, using the above schemes for the synthesis of bright attosecond pulses with a well-defined polarization state remains challenging.

In recent years, much attention was given to the so-called bielliptic or bicircular fields, in which the polarization of two copropagating beams, whose frequencies are usually related as 1:2 (ω - 2ω scheme), are, respectively, elliptical [16] or circular [17], whereas the electric field vector rotates in opposite directions. This field combination, according to the energy and spin angular momentum conservation, gives rise to circularly polarized harmonics, where, in the ω - 2ω scheme, the harmonics of orders $q = 3m - 1$ rotate right and the harmonics of orders $q = 3m + 1$ rotate left, whereas the $3m$ harmonics are, theoretically, completely suppressed. As a drawback of this scheme, it should be noted that the strong alternation of helicities between adjacent harmonics makes it difficult to synthesize ultrashort circularly polarized pulses. Furthermore, the harmonics emitted by this source, strictly speaking, are not exactly circularly polarized, but only on average. In fact, they are trains of linearly polarized attosecond pulses with alternating direction of polarization, and therefore cannot be directly used to probe the processes in chiral media on an attosecond timescale.

Despite the shortcomings described above, the existing sources of elliptically polarized XUV radiation present a new type of instrumentation, enabling diagnostics of magnetic and chiral media, as was demonstrated in a number of experiments [9,14,17,18]. At the same time, the intensity of an elliptically and circularly polarized high-harmonic radiation, especially in the so far poorly accessible region of photon energies of about 100 eV or higher, remains rather low, which still hinders the widespread use of sources of this type. Instead, synchrotron-type sources are currently most commonly used as sources of elliptically polarized radiation for applied research. In the sources based on bending magnets, the synchrotron radiation is known to be completely polarized; namely, within the plane of the electron orbit the radiation is linearly polarized, while for directions above or below this plane it is right or left elliptically polarized [19,20]. Due to this simple manipulation of polarization, such sources have been widely used to study the polarization- and helicity-sensitive response of various media [21–24]. However, the use of radiation pulses from storage rings in time-resolved measurements

is limited by the fact that they have too long (10–100 ps) duration and insufficient intensity to take snapshots of ultrafast chemical or physical processes. As an alternative, much brighter femtosecond sources based on free-electron lasers with various insertion devices such as undulators of special designs [25–29] that provide radiation with a high polarization ellipticity have recently been increasingly used for these purposes. However, the big advantage of the laboratory-scale sources based on HHG as compared to the large-scale facilities such as free electron lasers (FELs) is much higher accessibility to a wide scientific community.

As follows from the above considerations, the search for possibilities to efficiently amplify radiation from x-ray sources based on HHG is an important task. Recently, such a possibility was experimentally demonstrated for the case of the active medium of a plasma x-ray laser based on nickellike Kr^{8+} ions [30]. At the same time, since the gain of the active medium occurs only in a narrow frequency range around 32.8 nm wavelength, only one harmonic, resonant with a corresponding wavelength, was amplified, and its ellipticity was completely determined by the ellipticity of the seed radiation.

Our recent work [31] has shown the possibility to amplify attosecond pulses formed by a combination of linearly polarized HHs of an IR laser field in a hydrogenlike active medium of a plasma-based x-ray laser simultaneously irradiated with a replica of a fundamental-frequency IR field with the same linear polarization. Under the action of an intense IR field, due to the linear Stark effect caused by the degeneracy of the $|2s\rangle$ and $|2p\rangle$ states in the hydrogenlike ions, the gain spectrum of the active medium is redistributed from the frequency of the inverted transition to the sidebands whose frequencies are distant from the resonance by a multiple of the IR field frequency. Hence, if one of the HHs forming an attosecond pulse train is in resonance with one of the induced gain lines, then the remaining harmonics will automatically be in resonance with the other induced gain lines, separated from each other by twice the frequency of the IR field. However, because only two out of four energy degenerate states, corresponding to an excited energy level, experience the linear Stark effect, in the hydrogenlike medium the gain redistribution occurs only for the XUV or x-ray field with the same linear polarization as that of the modulating field (we choose the x -coordinate axis to be parallel to the propagation direction of both the XUV and IR fields, and the z axis to be parallel to the polarization direction of the IR field). For the XUV radiation with the orthogonal polarization (along the y axis) the gain remains localized at the (single) resonance frequency, which prevents the amplification of elliptically or circularly polarized harmonics.

Very recently, we have shown that amplification of sub-fs pulses of the radiation of a set of harmonics with an arbitrary elliptical (including circular) polarization is possible in a neonlike active medium of a plasma-based x-ray laser modulated by a linearly polarized IR laser field [32]. In this case, the major effect of the IR laser field is a fast (in a fraction of the optical cycle) shift of the energy levels of the resonant ions due to the quadratic Stark effect. As a result, unlike the case of a hydrogenlike active medium, the gain redistribution to combination frequencies occurs for the XUV or x-ray radiation with linear polarization both parallel and orthogonal to the polarization direction of the IR field. At a certain intensity of

the modulating field, the frequencies of the induced gain lines coincide for the z - and y -polarization components of the XUV or x-ray radiation, which makes it possible to amplify the set of circularly or elliptically polarized harmonics. In the case of a neonlike Ti^{12+} active medium, two characteristic regions are formed in the gain spectrum. In one of them, the gain for different polarization components of the XUV or x-ray radiation is almost the same, which makes it possible to amplify sub-fs pulse trains of HHs without significantly changing the shape, duration, and polarization of the pulses. At the same time, in the other part of the spectrum, the gain for one of the polarization components is considerably higher than for orthogonally polarized radiation, which allows one to control the harmonic ellipticity (and, in particular, to increase it).

In this work, we present a comprehensive theory of amplification process of elliptically or circularly polarized HHs, briefly discussed in [32]. We derive the analytical solution and, based on both the analytical and numerical studies, describe the evolution of an individual high harmonic with an arbitrary detuning from the resonance, a multiple of the doubled frequency of the modulating field, during its propagation through the medium. An evolution of a single harmonic with an arbitrary detuning was not considered in [32]. Analysis of this case is also crucial to understanding the amplification process of a set of harmonics. Then we analyze in detail the evolution of the selected sets of harmonics forming the trains of sub-fs pulses. The possibilities of the experimental implementation of this approach are discussed based on the specific example of an active medium of neonlike Ti^{12+} ions. The generation of radiation with a wavelength of 32.6 nm in a plasma of inverted Ti^{12+} ions was actively studied in [33–36] (see also review [37]), and the possibility of using neonlike Ti^{12+} ions to amplify the resonant high-order harmonic radiation with linear polarization was shown in [38]. The proposed approach could be experimentally implemented also in the plasma of other neonlike ions, where generation of XUV and x rays was widely studied; see [39–43] and reviews [37,44,45]. Moreover, amplification of HHs with an elliptical polarization via proposed technique should be potentially possible in plasmas of many nickellike ions, in particular, for Kr^{8+} ions (used in [30] to amplify the resonant harmonic of circular polarization), or Mo^{14+} and Ag^{19+} ions [46], as the fundamental scheme of energy levels in these ions is similar to the neonlike ions. Thus, potentially the results of this work could be extended to amplification of harmonics of elliptical or circular polarization at different wavelengths using plasma x-ray lasers based on various neonlike or nickellike active media.

This paper is organized as follows. The theoretical model is described in Sec. II. Section III presents an analytical solution for an individual high-order harmonic in a modulated neonlike active medium of a plasma-based x-ray laser, on the basis of which the optimal conditions are discussed for amplification of a single harmonic (a) with and (b) without significant change of polarization. Further, in Sec. IV and Sec. V, the results of numerical calculations are presented, which confirm the possibility of amplification and controlling the polarization state of a single harmonic (Sec. IV) or a combination of HHs (Sec. V) with elliptical or circular polarization. Finally, in Sec. VI the conclusions are given.

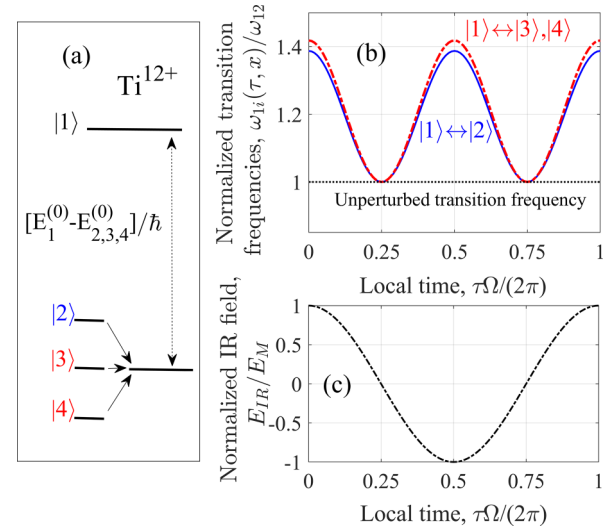


FIG. 1. (a) Relevant energy levels of Ti^{12+} ions corresponding to the states $|1\rangle = |3p^1 S_0, J = 0, M = 0\rangle$, $|2\rangle = |3s^1 P_1, J = 1, M = 0\rangle$, $|3\rangle = |3s^1 P_1, J = 1, M = 1\rangle$, and $|4\rangle = |3s^1 P_1, J = 1, M = -1\rangle$ (the states $|2\rangle$, $|3\rangle$, $|4\rangle$ are energy degenerate in the absence of the IR field). (b) Local-time dependence of the frequencies of inverted transitions $|1\rangle \leftrightarrow |2\rangle$ (blue solid curve) and $|1\rangle \leftrightarrow |3\rangle, |4\rangle$ (red dashed curve) calculated according to Eq. (4) under the action of the IR field with intensity 1×10^{17} W/cm², which is assumed in Figs. 3–17. The transition frequencies are normalized to the lasing frequency in the absence of the IR field, $\omega_{12}^{(0)} = (E_1^{(0)} - E_{2,3,4}^{(0)})/\hbar$, shown by black dotted curve. (c) Normalized IR field strength corresponding to panel (b).

II. THEORETICAL MODEL

Below we consider the amplification of the harmonics of the optical field in the active medium of a plasma-based x-ray laser with inversion at the $3p^1 S_0 - 3s^1 P_1$ transition of neonlike Ti^{12+} ions with the unperturbed resonance wavelength of 32.6 nm [33–38]. The scheme of energy levels of the $3p^1 S_0 - 3s^1 P_1$ transition of Ti^{12+} ions is shown in Fig. 1(a). The upper level is nondegenerate and corresponds to the state $|1\rangle$ with the total momentum value $J = 0$. The lower energy level is triply degenerate and corresponds to the $|2\rangle$, $|3\rangle$, and $|4\rangle$ states with $J = 1$ and the momentum projection on the quantization axis $M = 0, M = 1$, and $M = -1$, respectively. Further, we assume that the active medium has the form of a thin cylinder oriented along the x axis and use the spatially one-dimensional approximation implying that the characteristics of the medium and fields change only along the x axis.

The active medium of a plasma-based x-ray laser is irradiated with a resonant radiation from the seed of the XUV range, which at the input to the medium, $x = 0$, has the form

$$\vec{E}^{(\text{inc})}(t) = \frac{1}{2} [\vec{z}_0 \tilde{E}_z^{(\text{inc})}(t) + \vec{y}_0 \tilde{E}_y^{(\text{inc})}(t)] \exp(-i\omega t) + \text{c.c.}, \quad (1)$$

where \vec{z}_0 is unit vector along the z axis, ω is the carrier frequency of the XUV radiation, $\tilde{E}_z^{(\text{inc})}(t)$ and $\tilde{E}_y^{(\text{inc})}(t)$ are slowly varying complex amplitudes of the components of the incident field polarized along the z and y axes, respectively, and c.c. denotes a complex conjugate. We will further consider the amplification of quasimonochromatic resonant radiation (in Sec. III and Sec. IV), as well as the amplification of the set of

harmonics of the IR field that form a sequence of short pulses (in Sec. V). We also note that in Eq. (1) the phase difference between complex functions $\tilde{E}_z^{(\text{inc})}(t)$ and $\tilde{E}_y^{(\text{inc})}(t)$, as well as their relative amplitudes, can be arbitrary, which allows one to consider XUV radiation with an arbitrary (in the general case, elliptical) polarization.

In addition to XUV radiation, the active medium of a plasma-based x-ray laser is irradiated with an intense IR laser field propagating along the x axis and polarized along the z axis:

$$\tilde{E}_{IR}(x, t) = \tilde{z}_0 E_M \cos \left[\Omega \left(t - x \sqrt{\varepsilon_{pl}^{(IR)}} / c \right) \right]. \quad (2)$$

Here E_M and Ω are the amplitude and frequency of the IR field, c is the speed of light in vacuum, $\varepsilon_{pl}^{(IR)} = 1 - \omega_{pl}^2 / \Omega^2$ is the dielectric constant of the plasma for the modulating field, $\omega_{pl} = \sqrt{4\pi N_e e^2 / m_e}$ is the electron plasma frequency (hereinafter, the formulas are given in the CGS-ESU system), N_e is the concentration of free electrons in the plasma, and e and m_e are the charge and mass of the electron, respectively. In Eq. (2) the pulse duration of the IR field is assumed to be significantly longer than the duration of all the processes under study, which allows us to consider it monochromatic. In the case of Ti^{12+} ions, the frequency of a mid-IR laser field is at least two orders of magnitude lower than the frequency of any of the transitions connecting all four states $|1\rangle - |4\rangle$, shown in Fig. 1(a), with other ionic quantum states, as well as the transition frequencies from the upper state $|1\rangle$ to the lower states $|2\rangle$, $|3\rangle$, and $|4\rangle$ (while the transitions between those lower states are forbidden). As a result, the influence of the IR field on the $|1\rangle - |4\rangle$ states in such an adiabatic perturbation regime is reduced predominantly to a shift of the corresponding energy levels due to the quadratic Stark effect. In this case, the position of the i th energy level ($i = 1, 2, 3, 4$) is determined by [47]

$$E_i(x, t) = E_i^{(0)} + \frac{1}{2} \sum_{k \neq i} \frac{|d_{ki}^{(z)}|^2 E_M^2}{\hbar \omega_{ik}} \times \left\{ 1 + \cos \left[2\Omega \left(t - x \sqrt{\varepsilon_{pl}^{(IR)}} / c \right) \right] \right\}, \quad (3)$$

where $E_i^{(0)}$ is the unperturbed energy value, ω_{ik} is the unperturbed frequency of the transition from the i th state to the k th state, and $d_{ki}^{(z)}$ is the projection of the dipole moment of a given transition on the z axis. The summation in (3) is carried out over several dozens of states of the unperturbed (field-free) ion with the largest electric dipole moments of transitions to the state $|i\rangle$ (including the states $|1\rangle - |4\rangle$) [48].

We further introduce the notations $\Delta_E^{(i)} = \frac{1}{2} \sum_{k \neq i} \frac{|d_{ki}^{(z)}|^2 E_M^2}{\hbar \omega_{ik}}$ for the amplitude of the shift of the energy level corresponding to the i th state and $\Delta_\Omega^{(ij)} = (\Delta_E^{(i)} - \Delta_E^{(j)}) / \hbar$ for the amplitude of the frequency change of the $|i\rangle \leftrightarrow |j\rangle$ transition, where $i, j = 1, 2, 3, 4$. With the notations introduced, the instantaneous values of the frequencies of quantum transitions between the

$|1\rangle$, $|2\rangle$, $|3\rangle$, and $|4\rangle$ states can be represented as

$$\begin{aligned} \omega_{12}(\tau, x) &= \tilde{\omega}_{tr}^{(z)} + \Delta_\Omega^{(z)} \cos[2(\Omega\tau + \Delta Kx)], \\ \omega_{13}(\tau, x) &= \tilde{\omega}_{tr}^{(y)} + \Delta_\Omega^{(y)} \cos[2(\Omega\tau + \Delta Kx)], \\ \omega_{14}(\tau, x) &= \omega_{13}(\tau, x), \\ \omega_{23}(\tau, x) &= (\Delta_\Omega^{(z)} - \Delta_\Omega^{(y)}) \{1 + \cos[2(\Omega\tau + \Delta Kx)]\}, \\ \omega_{24}(\tau, x) &= \omega_{23}(\tau, x), \\ \omega_{34}(\tau, x) &= 0, \end{aligned} \quad (4)$$

where $\tau = t - x \sqrt{\varepsilon_{pl}^{(XUV)}} / c$ is the local time in the reference frame moving along the x axis with the phase velocity of the XUV radiation (1) in the plasma, $\varepsilon_{pl}^{(XUV)} = 1 - \omega_{pl}^2 / \omega^2$ is the dielectric constant of the plasma for the XUV radiation, $\Delta K = \Omega (\sqrt{\varepsilon_{pl}^{(XUV)}} - \sqrt{\varepsilon_{pl}^{(IR)}}) / c$ is an addition to the wave number of the modulating field due to the difference between its phase velocity and the XUV radiation phase velocity, $\tilde{\omega}_{tr}^{(z)} \equiv (E_1^{(0)} - E_2^{(0)}) / \hbar + \Delta_\Omega^{(z)}$ is the time-averaged $|1\rangle \leftrightarrow |2\rangle$ transition frequency, and $\tilde{\omega}_{tr}^{(y)} \equiv (E_1^{(0)} - E_3^{(0)}) / \hbar + \Delta_\Omega^{(y)} = (E_1^{(0)} - E_4^{(0)}) / \hbar + \Delta_\Omega^{(y)}$ is the time-averaged frequency of $|1\rangle \leftrightarrow |3\rangle$ and $|1\rangle \leftrightarrow |4\rangle$ transitions, $\Delta_\Omega^{(z)} \equiv \Delta_\Omega^{(12)}$, and $\Delta_\Omega^{(y)} \equiv \Delta_\Omega^{(13)} = \Delta_\Omega^{(14)}$. The superscripts (z) and (y) are used for the parameters of the transitions $|1\rangle \leftrightarrow |2\rangle$ and $|1\rangle \leftrightarrow |3\rangle, |4\rangle$, as they interact with the z - and y -polarization components of the XUV field, respectively.

Two important conclusions follow from Eqs. (3) and (4). First, unlike in an active medium of hydrogenlike ions [31], where the IR field linearly polarized along the z axis causes the linear Stark effect and leads to spatiotemporal modulation of frequencies of only those transitions, which are involved in the interaction with the z -polarized XUV or x-ray radiation, in a medium of neonlike Ti^{12+} ions, due to the quadratic Stark effect, the frequencies of transitions interacting with both the z -polarized and y -polarized components of the XUV radiation get modulated. Second, in the presence of a modulating IR field, both the average values and the amplitudes of the frequency shift of the $|1\rangle \leftrightarrow |2\rangle$ and $|1\rangle \leftrightarrow |3\rangle, |4\rangle$ quantum transitions interacting with z - and y -polarized components of XUV radiation are different [see Fig. 1(b)] since the states $|2\rangle$ and $|3\rangle, |4\rangle$ experience different energy shifts due to the IR field-induced quadratic Stark effect.

The coupled space-time evolution of the XUV radiation and the quantum state of Ti^{12+} ions in the presence of the IR field (2) is described in Appendix A. These equations were presented in less detail in [32].

III. AMPLIFICATION AND CONTROL OF THE ELLIPTICITY OF AN INDIVIDUAL HIGH HARMONIC: ANALYTICAL SOLUTION

First of all, let us consider the analytical solution for the polarization components of the XUV radiation in a medium, $\tilde{E}_z(x, \tau)$ and $\tilde{E}_y(x, \tau)$, derived in a linear approximation (see [49]), and implying that (i) during the considered time interval the population of states (the density matrix diagonal elements) does not change, $\tilde{\rho}_{ii}(x, \tau) = \tilde{\rho}_{ii}(x, \tau = 0)$, $i = 1, 2, 3, 4$, (ii) the coherences on the dipole-forbidden transitions

between the $|2\rangle$, $|3\rangle$, and $|4\rangle$ states are identically equal to zero [which is a consequence of the approximation (i)], and (iii) the coherences at the dipole-allowed $|1\rangle \leftrightarrow |2\rangle$, $|1\rangle \leftrightarrow |3\rangle$, and $|1\rangle \leftrightarrow |4\rangle$ transitions are equal to zero before the arrival of the XUV field, which corresponds to neglecting the spontaneous emission of the medium. The first two approximations are valid for not very large values of local time τ and not very high intensity of the seed. At the same time, the third approximation implies that the intensity of the seed is high enough to neglect the spontaneous emission of the medium. These approximations are compatible with each other as is confirmed by the results of the numerical integration of the nonlinear system of Eqs. (A4) and (A7) (see Appendix A), which are presented in the next section.

To derive an analytical solution, we assume that the seeding radiation (1) is a single monochromatic high-order harmonic at the frequency ω with the following polarization amplitudes:

$$\tilde{E}_z^{(\text{inc})}(\tau) = E_0^{(z)} \text{ and } \tilde{E}_y^{(\text{inc})}(\tau) = E_0^{(y)}, \quad (5)$$

where $E_0^{(z)}$ and $E_0^{(y)}$ are complex numbers. As shown in Appendix B, if the frequency of the XUV radiation (1) coincides with the time-average frequency of the $|1\rangle \leftrightarrow |2\rangle$ transition or is tuned from it to an even multiple of the modulation frequency: $\omega = \bar{\omega}_{tr}^{(z)} + 2k\Omega$, where k is an integer, the z -polarization component of the XUV radiation will be resonantly amplified:

$$\tilde{E}_z = E_0^{(z)} \exp[g_k^{(z)}(P_\Omega^{(z)})x], \quad (6a)$$

$$g_k^{(z)}(P_\Omega^{(z)}) = g_{\text{total}}^{(z)} J_k^2(P_\Omega^{(z)}), \quad (6b)$$

where $g_k^{(z)}(P_\Omega^{(z)})$ is the effective gain of the z -polarized radiation with frequency $\omega = \bar{\omega}_{tr}^{(z)} + 2k\Omega$, $g_{\text{total}}^{(z)} = \frac{2\pi\omega N_{\text{ion}} n_{tr}^{(z)} d_z^2}{\hbar c \gamma_z \sqrt{\epsilon_{pl}^{(XUV)}}}$ is the gain of z -polarized radiation in the absence of modulation (the gain in intensity is two times higher, $G_{\text{total}}^{(z)} = 2g_{\text{total}}^{(z)}$), $\gamma_z \equiv \gamma_{12}$, and $n_{tr}^{(z)} = \tilde{\rho}_{11}(x, \tau) - \tilde{\rho}_{22}(x, \tau)$ is the population difference at the transition $|1\rangle \leftrightarrow |2\rangle$; in the approximation under consideration, $n_{tr}^{(z)} = 1$, $J_k(x)$ is the Bessel function of the first kind of order k , and $P_\Omega^{(z)} = \frac{\Delta_\Omega^{(z)}}{2\Omega}$ is the frequency modulation index of the $|1\rangle \leftrightarrow |2\rangle$ transition under the influence of the IR field (due to the quadratic Stark effect).

Similarly to z -polarized radiation, the y -polarized component of the XUV field is amplified most efficiently if the frequency of the field coincides with the $|1\rangle \leftrightarrow |3\rangle$, $|4\rangle$ transition frequency or is tuned from it by an even multiple of the modulation frequency: $\omega = \bar{\omega}_{tr}^{(y)} + 2k'\Omega$, where k' is an integer. In this case, the solution for \tilde{E}_y has the form (6) up to a replacement of the indices $z \rightarrow y$ and $k \rightarrow k'$:

$$\tilde{E}_y = E_0^{(y)} \exp[g_{k'}^{(y)}(P_\Omega^{(y)})x], \quad \text{where} \quad (7a)$$

$$g_{k'}^{(y)}(P_\Omega^{(y)}) = g_{\text{total}}^{(y)} J_{k'}^2(P_\Omega^{(y)}). \quad (7b)$$

Here $g_{k'}^{(y)}(P_\Omega^{(y)})$ is the effective gain of the y -polarized radiation with frequency $\omega = \bar{\omega}_{tr}^{(y)} + 2k'\Omega$, $g_{\text{total}}^{(y)} = \frac{4\pi\omega N_{\text{ion}} n_{tr}^{(y)} d_y^2}{\hbar c \gamma_y \sqrt{\epsilon_{pl}^{(XUV)}}}$ is the gain (in the field amplitude) in the absence of modulation (the gain in intensity is equal to $G_{\text{total}}^{(y)} = 2g_{\text{total}}^{(y)}$), $n_{tr}^{(y)} = \tilde{\rho}_{11}(x, \tau) - \tilde{\rho}_{33}(x, \tau) = \tilde{\rho}_{11}(x, \tau) - \tilde{\rho}_{44}(x, \tau)$ is the population difference at the $|1\rangle \leftrightarrow |3\rangle$, and $|1\rangle \leftrightarrow |4\rangle$ transitions, which in the case under consideration is the same and equal

to $n_{tr}^{(y)} = 1$, $\gamma_y \equiv \gamma_{13} = \gamma_{14}$, and $P_\Omega^{(y)} = \frac{\Delta_\Omega^{(y)}}{2\Omega}$ is the index of modulation of the $|1\rangle \leftrightarrow |3\rangle$, $|4\rangle$ transition frequencies.

Due to the fact that under the influence of a modulating field, the frequencies of $|1\rangle \leftrightarrow |2\rangle$ and $|1\rangle \leftrightarrow |3\rangle$, $|4\rangle$ quantum transitions become different, in the general case, the conditions for resonant amplification of z - and y -polarized radiation do not coincide. However, in order for the elliptically or circularly polarized radiation to be amplified, both of its polarization components must be amplified simultaneously. This is possible if $\omega = \bar{\omega}_{tr}^{(z)} + 2k\Omega = \bar{\omega}_{tr}^{(y)} + 2k'\Omega$, i.e., the difference between the frequencies $\bar{\omega}_{tr}^{(z)}$ and $\bar{\omega}_{tr}^{(y)}$ must be equal to or a multiple of twice the frequency of the modulating field: $\bar{\omega}_{tr}^{(y)} - \bar{\omega}_{tr}^{(z)} = 2\Omega(k-k')$. We further consider the case that is easiest for experimental implementation:

$$\bar{\omega}_{tr}^{(y)} - \bar{\omega}_{tr}^{(z)} = 2\Omega. \quad (8)$$

In this case, $k' = k-1$, and if the effective gain of the z component of the radiation is proportional to $J_k^2(P_\Omega^{(z)})$, then the gain of the y component of the radiation is proportional to $J_{k-1}^2(P_\Omega^{(y)})$. Due to the fact that $\bar{\omega}_{tr}^{(y)} - \bar{\omega}_{tr}^{(z)} = \Delta_\Omega^{(y)} - \Delta_\Omega^{(z)}$ and $\Delta_\Omega^{(y)} - \Delta_\Omega^{(z)} \sim E_M^2$ [see Eq. (3)], the equality (8) unambiguously relates the intensity of the modulating field to its frequency and wavelength. For Ti^{12+} ions, this dependence is shown in Fig. 2(a), where, in addition to the wavelength of the modulating field, for which the condition (8) is satisfied (left vertical axis), the ionization rates from the $|1\rangle - |4\rangle$ states, $w_{\text{ion}}^{(i)}$, are shown versus the intensity of the modulating field (right vertical axis). The ionization rates are normalized to the half-width of the gain line in the absence of a modulating field, $\gamma_{12}^{(0)}$. For the resonant polarization of the medium to have a time to develop, it is necessary to fulfill the condition $w_{\text{ion}}^{(i)} < \gamma_{12}^{(0)}$ that limits the maximum intensity of the modulating field and its minimum wavelength. It is worth to note that the ionization rates were calculated using the Perelomov-Popov-Terent'ev formula [50], which has limited accuracy for states of multiply charged ions. In the following, we will estimate the values of maximum intensity and minimum wavelength of the modulating field as 1×10^{17} W/cm² and 3.2 μm , respectively.

Figure 2(b) shows the position of the induced gain lines of the active medium, $\omega_k = \bar{\omega}_{tr}^{(z)} + 2k\Omega$, with substantially nonzero gain coefficients $g_k^{(z)}(P_\Omega^{(z)})$ [see Eq. (6b)] under the condition (8) as a function of the intensity of the modulating field [the wavelength of the modulating field is different for each value of its intensity and varies along the blue solid curve in Fig. 2(a)]. As follows from Fig. 2(b), a coordinated change in intensity and wavelength of the modulating field allows to change the absolute location of the induced gain lines and makes it possible to tune them to the desired frequencies (thus allowing for the amplification of either a single-frequency or a multifrequency seeding XUV field). Besides, the spectrum of the induced gain lines may be rather broad, and its width can be a significant fraction of the inverted transition frequency.

We further consider the modulation of the active medium by an IR field with a wavelength of 3.2 μm and intensity of 1×10^{17} W/cm². In recent years, a number of novel approaches have been proposed that allow achieving such intensities with optical parametric sources in the mid-IR range

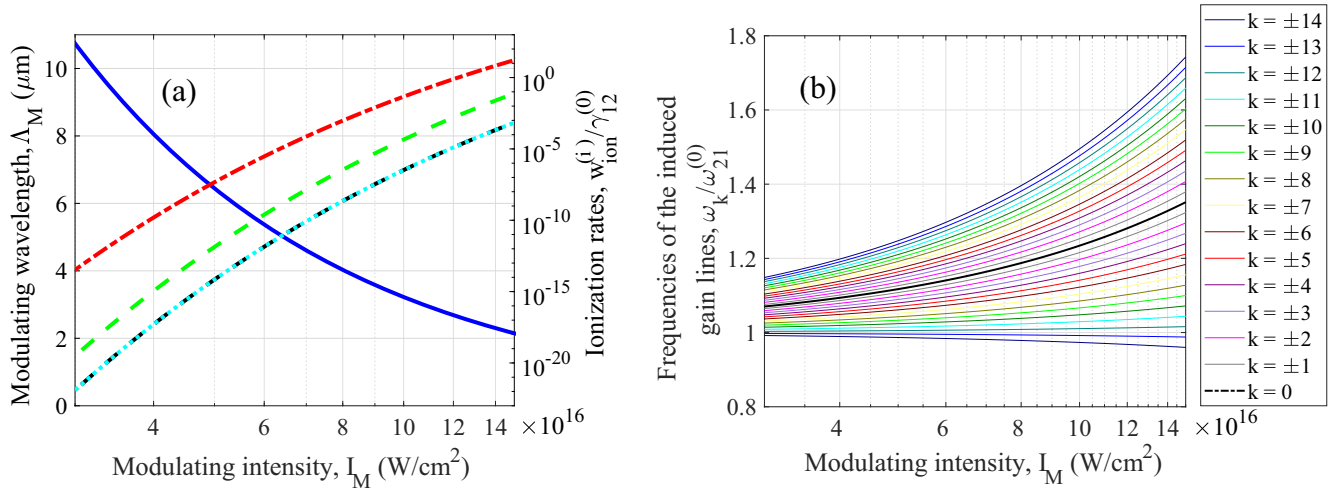


FIG. 2. (a) Dependences of (i) the wavelength of the modulating field for which the condition (8) is satisfied (blue solid curve, left vertical axis) and (ii) ionization rates from the resonant states of Ti^{12+} ions normalized to the half-width of the transition line in the absence of a field (other curves, right vertical axis) on the intensity of the modulating field. Red dash-dotted curve corresponds to the ionization rate from the $|1\rangle$ state, green dashed curve—from the $|2\rangle$ state, and the identical (overlapping) black and turquoise dashed curves—to the ionization rates from the $|3\rangle$ and $|4\rangle$ states. (b) The frequencies of the induced gain lines of the active medium, $\omega_k = \bar{\omega}_{tr}^{(z)} + 2k\Omega$, for different $-14 \leq k \leq 14$ under the condition (8) as a function of the intensity of the modulating field [as the intensity changes, the wavelength of the modulating field varies along the blue curve in Fig. 2(a)]. The frequencies of the induced gain lines are normalized to the inverted transition frequency in the absence of the modulation, $\omega_{21}^{(0)} = (E_1^{(0)} - E_{2,3,4}^{(0)})/\hbar$. Bold dash-dotted black curve corresponds to the central frequency of the inverted transition for z -polarization component of the XUV field, $\bar{\omega}_{tr}^{(z)}$. Colored thin curves correspond to the sidebands in the gain spectrum. The colors are indicated in the figure legend.

[51–54]. This combination of the IR field wavelength and intensity corresponds to the widest spectrum of matched gain lines for the orthogonal polarization components of the XUV field (8), which makes it possible to amplify the shortest XUV pulses formed by a set of elliptically or circularly polarized high harmonics. In this case, the inverse ionization rate from the $|1\rangle$ state is equal to $1/w_{\text{ion}}^{(1)} \approx 4.6$ ps, and the time-averaged $|1\rangle \leftrightarrow |2\rangle$ transition frequency coincides with the frequency of 133rd harmonic of the modulating field, $\bar{\omega}_{tr}^{(z)} = 133 \times \Omega$. The wavelength of resonant radiation in vacuum in this case is equal to $\lambda_{\text{HI}133} = 24.34$ nm. Note that this is a calculated value obtained from the available theoretical data on the positions of the energy levels of Ti^{12+} ions and the rates of radiation transitions between them [48]. According to these data, in the absence of a modulating field, the wavelength of the resonant XUV radiation is 30.04 nm, whereas in the experiment, the central wavelength of the generated radiation is 32.63 nm. This difference should be kept in mind when planning an experiment. As follows from the solutions given by Eqs. (6) and (7), the effective gain coefficients for the z - and y -polarized components of the XUV field are proportional to the squares of the Bessel functions, the order of which is determined by the detuning of the field frequency from the central frequencies of the transitions $\bar{\omega}_{tr}^{(z)}$ and $\bar{\omega}_{tr}^{(y)}$, respectively. We also note that in the linear amplification regime, under the condition $n_{tr}^{(y)} = n_{tr}^{(z)}$, the equality $g_{\text{total}}^{(y)} \simeq g_{\text{total}}^{(z)} \equiv g_{\text{total}}$ holds due to the facts that $\gamma_y \simeq \gamma_z \equiv \gamma_{tr}$ (up to a difference in the ionization rates from the $|2\rangle$ and $|3\rangle$, $|4\rangle$ states) and $2d_y^2 = d_z^2$. As a result, the difference between the effective gains for the y - and z -polarized components of the XUV radiation is solely due to the difference in the orders and arguments of the Bessel

functions in Eqs. (6b) and (7b). For the indicated intensity and wavelength of the IR field, the modulation indices for the $|1\rangle \leftrightarrow |2\rangle$ and $|1\rangle \leftrightarrow |3\rangle$, $|4\rangle$ transitions are $P_{\Omega}^{(z)} \approx 12.57$ and $P_{\Omega}^{(y)} \approx 13.57$, respectively.

The corresponding gain spectra for the z - and y -polarized components of the XUV radiation [dependences of the effective gains $g_k^{(z)}(P_{\Omega}^{(z)})$ and $g_{k-1}^{(y)}(P_{\Omega}^{(y)})$ on $k = \frac{\omega - \bar{\omega}_{tr}^{(z)}}{2\Omega}$] are shown in Fig. 3. Due to the fact that, at the same field frequency ω , the z component of the field is in resonance with the k th induced gain line of the active medium, and the y component of the field is in resonance with the $(k-1)$ -th gain line, and also due to the differences in the modulation indices for the $|1\rangle \leftrightarrow |2\rangle$ and $|1\rangle \leftrightarrow |3\rangle$, $|4\rangle$ transitions, the gain coefficients for the z and y components of the XUV radiation are different. In this case, depending on the value of k , any of three options is possible: (a) $g_k^{(z)}(P_{\Omega}^{(z)}) \approx g_{k-1}^{(y)}(P_{\Omega}^{(y)})$, (b) $g_k^{(z)}(P_{\Omega}^{(z)}) > g_{k-1}^{(y)}(P_{\Omega}^{(y)})$, and (c) $g_k^{(z)}(P_{\Omega}^{(z)}) < g_{k-1}^{(y)}(P_{\Omega}^{(y)})$. In the first case, the polarization components of the XUV radiation are amplified with equal efficiency, which makes it possible to amplify elliptically or circularly polarized radiation while maintaining the degree of ellipticity. In case (b), z -polarized radiation is amplified more efficiently than y -polarized radiation. As a result, as the field propagates through the medium, the ellipticity of the field changes due to the change in the relative amplitudes of the polarization components. If quasimonochromatic XUV radiation with low ellipticity and the major axis of the polarization ellipse parallel to the y axis, which can be obtained via the HHG process driven by an elliptically polarized laser field, enters the medium, then, as it is amplified in the medium, the ellipticity of the XUV radiation will increase, and at a certain

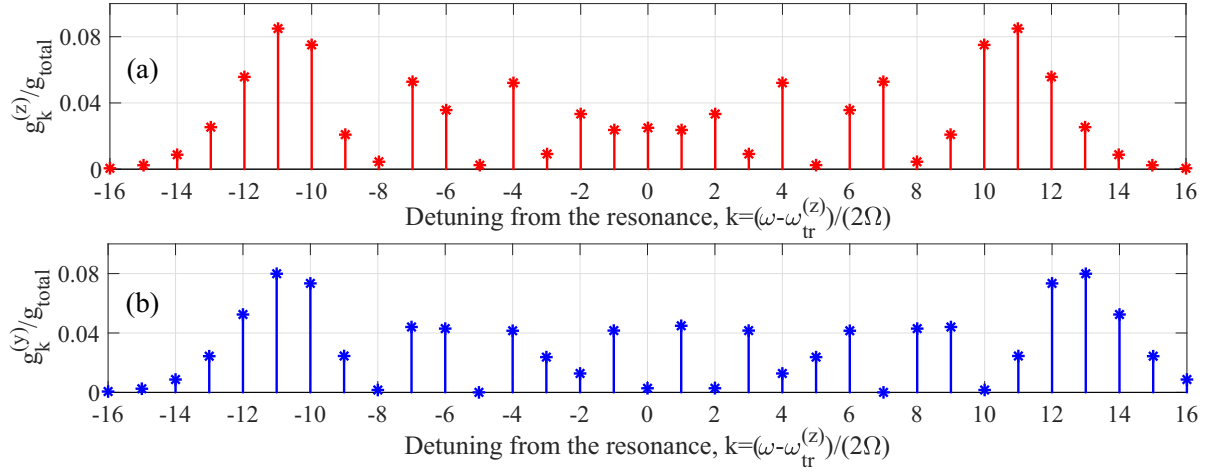


FIG. 3. Dependences of the effective gain coefficients (6b) and (7b) for the XUV radiation of z polarization (a) and y polarization (b), on the k number, which corresponds to the detuning of the radiation frequency from resonance with a time-averaged $|1\rangle \leftrightarrow |2\rangle$ transition frequency. Effective gain factors are normalized to the gain in the absence of modulation, g_{total} . Here $P_{\Omega}^{(z)} \approx 12.57$ and $P_{\Omega}^{(y)} \approx 13.57$.

position inside the medium, its polarization will become close to circular. However, if the major axis of the polarization ellipse of the XUV radiation at the entrance to the medium coincides with the z axis, its ellipticity will decrease during propagation in the medium, and the polarization of the output radiation will approach linear. In case (c), reasoning similar to case (b) holds up to 90° rotation of the polarization ellipse of the incident field. It should be noted that according to the solutions (6) and (7) derived above, both polarization components of the XUV radiation are amplified independently of each other, while the phase relations between them are preserved.

The appearance of multiple induced gain lines allows one either to amplify a train of sub-fs pulses constituted by a set of HHs of (a replica of) the modulating IR field, as was discussed in [32], or to choose a proper induced gain line for the amplification of a single high-order harmonic of an auxiliary laser field (with a frequency not a fraction, neither a multiple of the frequency of the modulating field). In the latter case, the choice of the gain line might allow controlling the polarization state of the amplified harmonic, which is impossible in the absence of the modulation [30]. Besides, by changing the parameters (intensity and wavelength) of the modulating IR field it is possible to tune the proper induced gain line in resonance with the desired high-order harmonic.

As can be seen from Fig. 3, gain factors for z - and y -polarized radiation for $-14 \leq k \leq -6$ are nearly equal. Accordingly, the gain lines with k inside this region are most suitable for amplifying radiation of elliptical or circular polarization while maintaining its polarization state. Below we consider the case $k = -10$ for amplifying a single harmonic, and, similarly to [32], but in more detail, the case $k = -13, -12, -11, -10$, and -9 for a set of five harmonics forming a sequence of the shortest (for the considered medium) pulses of circular polarization. At the same time, as follows from Fig. 3, for positive values of k , maximum gain anisotropy is achieved. Further, we will also consider the case $k = 10$, in which the gain for the z -polarized radiation is close to the maximum and the gain for the y -polarized radiation is almost zero. These conditions are optimal for enhancing the harmonic field

ellipticity in the process of its amplification. In addition, similarly to [32], we will consider the case of amplification of a set of five high-order harmonics of elliptical polarization, which are in resonance with induced gain lines that correspond to $k = -3, -1, 1, 3$, and 5 . For all the aforementioned gain lines, the y -polarized radiation is amplified more strongly than the z -polarized radiation, which allows one to consistently change the ellipticity of the set of high harmonics.

IV. NUMERICAL RESULTS FOR THE AMPLIFICATION OF A SINGLE ELLIPTICALLY OR CIRCULARLY POLARIZED HIGH-ORDER HARMONIC

We will characterize the ellipticity of the XUV radiation by the quantity σ [55]:

$$\sigma = \tan(\chi), \quad (9)$$

where the angle χ is determined as

$$\sin(2\chi) = \frac{2|\tilde{E}_z||\tilde{E}_y|\sin(\delta)}{|\tilde{E}_z|^2 + |\tilde{E}_y|^2}, \quad (10)$$

and $\delta \equiv \arg(\tilde{E}_z) - \arg(\tilde{E}_y)$ is the phase difference between the slowly varying field amplitudes \tilde{E}_z and \tilde{E}_y .

In what follows, we will consider the amplification of circularly and elliptically polarized XUV fields with $\delta = \pi/2$, both (z - and y -) polarization components of which are tuned to exact resonance with the corresponding gain lines. In this case, the quantities $g_k^{(z)}$ and $g_{k-1}^{(y)}$ are real, and if the principal axes of the polarization ellipse of the incident field coincide with the y and z axes, their orientation will not change during amplification. The ellipticity of the output radiation for this case is determined by a ratio of amplitudes of its polarization components.

In the following, we consider an active medium with free-electron density $N_e = 5 \times 10^{19} \text{ cm}^{-3}$ and a density of neonlike Ti^{12+} ions $N_{\text{ion}} \approx 4.2 \times 10^{18} \text{ cm}^{-3}$. Among these ions approximately 1% are in the $|1\rangle$ state at $\tau = 0$ (the initial population of the $|2\rangle - |4\rangle$ states is close to zero due to their

rapid radiation depletion). In this case, the small signal gain (in intensity) for the resonant XUV radiation in the absence of modulation will be about $G_{\text{total}}^{(0)} = 70 \text{ cm}^{-1}$. The inverse collision rate, evaluated from the experimentally measured spectral width of the gain line of an optically thin medium, $\Delta\lambda/\lambda = 1.5 \times 10^{-4}$, is $1/\gamma_{\text{Coll}} = 213 \text{ fs}$. The times of tunneling ionization from the $|1\rangle - |4\rangle$ states under the action of a modulating field with an intensity of $1 \times 10^{17} \text{ W/cm}^2$ are $1/w_{\text{ion}}^{(1)} \approx 4.6 \text{ ps}$, $1/w_{\text{ion}}^{(2)} \approx 4.7 \text{ ns}$, and $1/w_{\text{ion}}^{(3)} = 1/w_{\text{ion}}^{(4)} \approx 65 \text{ }\mu\text{s}$. It is worth to note that for the considered plasma parameters the frequency of the IR field, $\Omega = 5.8 \times 10^{14} \text{ s}^{-1}$, is close to the plasma frequency of the active medium with the relativistic correction, $\omega_{\text{pl}}^{(\text{rel})} = \omega_{\text{pl}}/\sqrt{\gamma} = 3.6 \times 10^{14} \text{ s}^{-1}$, where $\gamma \approx 1.2$ is the Lorentz factor of an electron in the IR field. It could lead to an electron pileup creation by the ponderomotive force at the leading edge of the IR pulse [56,57], resulting in a partial IR field reflection. However, since we consider rather long (a few picosecond) IR pulses (the IR field is effectively monochromatic), the transient effects at the front edge of the pulse can be neglected.

In contrast to the analytical approach, which assumed a monochromatic XUV radiation to be amplified, numerical calculations are performed for the case of a smooth envelope given by

$$\begin{aligned} \tilde{E}_z^{(\text{inc})}(\tau) &= E_0^{(z)}[\theta(\tau) - \theta(\tau - \tau_{\text{zero}})]\sin^2(\pi\tau/\tau_{\text{zero}}), \\ \tilde{E}_y^{(\text{inc})}(\tau) &= E_0^{(y)}[\theta(\tau) - \theta(\tau - \tau_{\text{zero}})]\sin^2(\pi\tau/\tau_{\text{zero}}), \end{aligned} \quad (11)$$

where the parameter τ_{zero} determines the duration of the seed field envelope from zero to zero. In further calculations, we assume $\tau_{\text{zero}} = 750 \text{ fs}$. In this case, the full width at half-maximum (FWHM) of the intensity envelope is about 270 fs. These values of the parameters were chosen from the consideration that for effective amplification of the incident field, its duration should exceed the transient time for resonant polarization of the active medium, which in our case is about 200 fs. To amplify shorter pulses, it is necessary to shorten the polarization transient time by (i) increasing the collisional relaxation rate γ_{Coll} (using a denser and/or hotter plasma [58,59]) or (ii) increasing the ionization rates $w_{\text{ion}}^{(i)}$, $i = 1, 2, 3, 4$ (using a more intense modulating field). In both cases, however, the broadening of the gain spectrum of the active medium will be accompanied by a decrease in its peak value. Another possibility for amplifying short pulses is to use high-intensity seed radiation, in the presence of which relaxation processes in the active medium can be neglected (see the section in [31] where the separation of a single attosecond pulse from a train is addressed). However, the consideration of this amplification regime is beyond the scope of this article. Further, we will consider the case of a seeding radiation with the intensity of polarization components in the range of $10^6 - 10^8 \text{ W/cm}^2$; in this case, for the considered lengths of the medium (up to 15 mm), the amplification of radiation occurs in a regime close to linear.

A. Ellipticity-increasing amplification of an individual harmonic

Here we consider amplification of the 153rd harmonic ($\lambda_{\text{H153}} = 21.14 \text{ nm}$) of the modulating field; this harmonic is resonant to the induced gain lines with $k = 10$ (for z

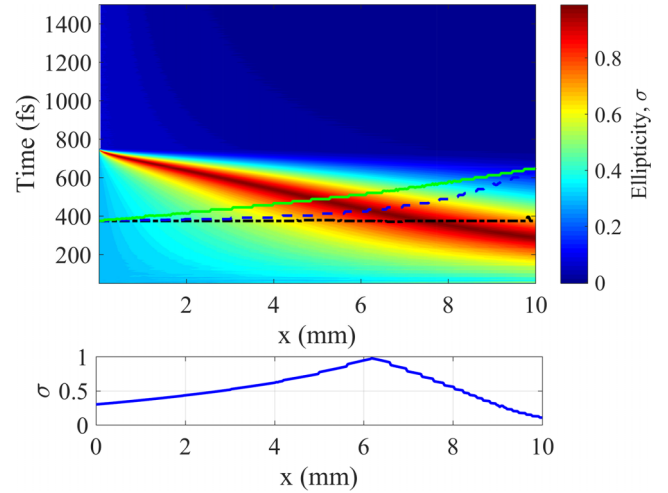


FIG. 4. Top panel: Space-time dependence of ellipticity, σ , of 153rd harmonic of the modulating field ($k = 10$). At the entrance to the medium, $\sigma(x = 0) = 0.3$ (y -polarization dominates). Green solid and black dash-dotted curves show the positions of the envelope maxima of the z - and y -polarization components of the amplified radiation, respectively. Blue dashed curve shows the maximum of the total intensity of the polarization components. For visibility, we don't show the interval $0 \leq \tau \leq 50 \text{ fs}$, where the ASE dominates over the amplified signal. Bottom panel: Ellipticity of the XUV radiation at the maximum of the total intensity of its polarization components as a function of the length of the medium, x .

polarization) and $(k-1) = 9$ (for y polarization). As already mentioned, in this case, the gain for the z component of the XUV radiation is close to maximum, whereas the gain for the y component is minimum, which makes it possible to effectively control the ellipticity of the radiation during its amplification.

The top panel of Fig. 4 shows the dependence of the amplified radiation ellipticity (9) on the local time τ and the spatial coordinate x (length of the active medium). The intensities of the y and z components of the seed radiation are assumed to be 10^7 W/cm^2 and $0.9 \times 10^6 \text{ W/cm}^2$, respectively. Accordingly, at $x = 0$ and $0 \leq \tau \leq 750 \text{ fs}$, the radiation ellipticity is 0.3, and the y polarization is dominant (at later times, the incident field is zero). As the radiation propagates in the medium, its ellipticity increases as a result of the predominant amplification of the z -polarized component, but this growth occurs nonuniformly in time; see Fig. 5, which shows the intensity time dependences [Fig. 5(a)] as well as the amplitude spectra [Fig. 5(b)] of the polarization components of the XUV field at different lengths of the medium. The amplification of the z -polarized field proceeds in a regime close to linear (without a significant change of the population difference in the medium) and is accompanied by a narrowing of its spectrum [see Fig. 5(b)] as well as a lengthening of its envelope [see Fig. 5(a)]. Thus, for an arbitrary length of the medium, a time interval appears, during which the z -polarized radiation component becomes more intense than its y -polarized counterpart, so that there is a moment of time at which the ellipticity of radiation approaches unity; see the top panel of Fig. 4 and the inset in Fig. 5(a), showing the cuts of Fig. 4 for a few fixed propagation distances. For small lengths, the

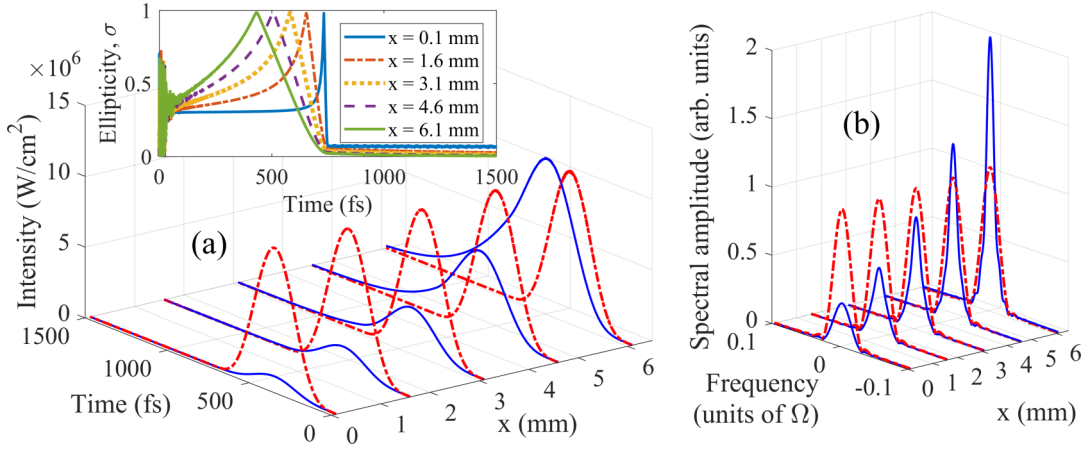


FIG. 5. (a) Dependences of the intensities of the polarization components of the XUV field on the local time, τ , corresponding to Fig. 4, at different lengths of the medium: $x = 0.1$ mm, 1.6 mm, 3.1 mm, 4.6 mm, and 6.1 mm. Red dash-dotted curve corresponds to the y -polarization component of the field, while blue solid curve shows the z component. The inset shows the time dependences of ellipticity of the field at the same lengths of the medium. For a larger length, the peak of ellipticity shifts to an earlier time. The noiselike time dependence of the ellipticity at the very initial times is caused by the ASE. (b) Spectral amplitudes of the polarization components of the XUV field at the same propagation distances through the medium. Red dash-dotted curve and lower gain correspond to the y component of the field; blue solid curve and higher gain correspond to the z component. The curves are normalized to the peak amplitude of the Fourier transform of the y component of the seeding radiation.

z -polarized component dominates at the very end of the pulse (near $\tau = 750$ fs), where the y -polarized field tends to zero, whereas the z component is nonzero due to amplification. As the length of the medium increases, the z -polarized radiation becomes comparable in amplitude with the y -polarized one at earlier moments of the local time. As a result, the area of maximum ellipticity shifts to the maximum of the field envelope. It should be noted that the maxima of the envelopes of the z - and y -polarized fields coincide only at $x = 0$, since in the process of amplification, the maximum of the envelope of the z component shifts towards later moments of local time.

The spatial dependence of the positions of the maxima of the z - and y -field components is shown on the top panel in Fig. 4 with green solid and black dash-dotted curves. In addition, the blue dashed curve in Fig. 4 shows the position of the maximum of the total intensity of the polarization components: in a thin medium, the maximum of the total intensity is achieved near the maximum of the y -polarized field envelope (z -polarized component is weaker), while at the maximum considered medium length, the maximum of the total intensity shifts to the maximum of the envelope of z -polarized field, which becomes dominant due to its strengthening discussed above.

The bottom panel of Fig. 4 shows the spatial dependence of the field ellipticity at the time instant corresponding to the maximum of the total intensity of its polarization components. As can be seen, with an increase of the medium length, the field ellipticity increases due to an increase of the amplitude of the z -polarized component. At $x \approx 6.1$ mm, the radiation at the maximum of the envelope of the total intensity of both polarization components acquires polarization approaching circular, $\sigma \simeq 1$, while for larger lengths of the medium, the output ellipticity decreases because of a further increase of the amplitude of the z -polarized field. At the optimal length

of the medium, $x = 6.1$ mm, the peak intensities of the z and y components of the field are approximately equal, but the energy contained in the z component turns out to be much larger due to an increase in its duration during amplification.

We also note that for the considered intensity of the incident field ($\sim 10^7$ W/cm²), the energy of the amplified spontaneous emission (ASE) from the active medium is insignificantly small compared to the amplified HH signal. The only manifestation of the ASE is a change of ellipticity of the radiation at the very initial moments of time, $\tau \leq 50$ fs (before the HH signal becomes noticeable); see the inset in Fig. 5(a). Figures 4 and 5 demonstrate that the use of a modulated active medium of a plasma-based x-ray laser makes it possible to increase the ellipticity of a single harmonic by more than three times with a simultaneous increase in the radiation energy by 2.7 times.

B. Polarization-maintaining amplification of a circularly polarized single harmonic

We will now consider the amplification of the 113th harmonic ($\lambda_{H113} = 28.66$ nm) of the modulating field; this harmonic is resonant to the induced gain lines with $k = -10$ (for z polarization) and $(k-1) = -11$ (for y polarization). In this case, the gain factors for different polarization components are close to each other (see Fig. 3), which makes it possible to amplify the circularly or elliptically polarized radiation without a noticeable change in its polarization state. We will consider the case of a circularly polarized field ($\sigma = 1$); at the entrance to the medium, the peak intensities of the z - and y -polarized components coincide and are equal to 10^7 W/cm².

The space-time dependence of the ellipticity of the amplified radiation is shown in Fig. 6 (top panel), where the green solid curve also marks the position of the maximum of the

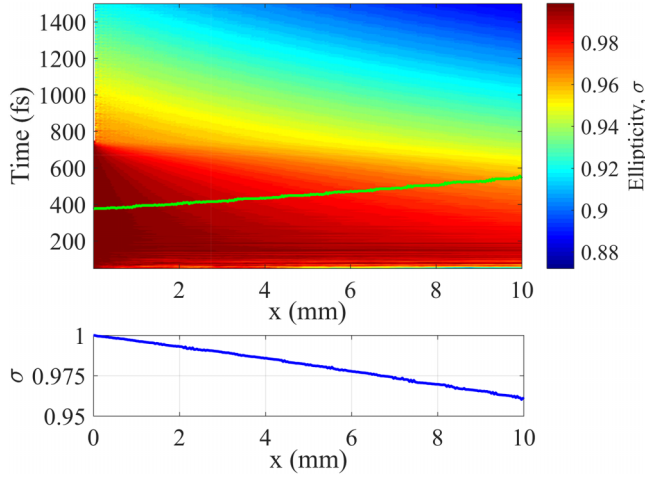


FIG. 6. Top panel: Space-time dependence of ellipticity, σ , of 113th harmonic of the modulating field ($k = -10$). The incident radiation is circularly polarized, $\sigma(x=0) = 1$. Green solid curve shows the positions of the maxima of the envelopes of the z - and y -polarized components of the field (they coincide on the scale of the figure). For visibility, we don't show the interval $0 \leq \tau \leq 50$ fs, where the ASE dominates over the amplified signal. Bottom panel: Ellipticity of XUV radiation at the maximum of the total intensity of its polarization components as a function of the length of the medium, x .

radiation intensity envelope (the maxima of the envelopes of different polarization components coincide on the scale of the figure). The bottom panel of Fig. 6 shows the field ellipticity at the maximum of its envelope versus the length of the medium. As follows from Fig. 6, the field ellipticity decreases monotonically with an increase of the medium length due to a slightly different amplification of its polarization components

(the z component is amplified somewhat more strongly). Nevertheless, even for the maximum considered length of the medium, the radiation retains its polarization close to circular: $\sigma \approx 0.96$ for $x = 10$ mm.

The time dependences of the intensities of the polarization components of the field and the corresponding spectra at different lengths of the medium are shown in Fig. 7(a) and Fig. 7(b), respectively. As can be seen from Fig. 7(a), in the course of amplification, the field peak intensity increases by approximately 20 times, while its energy increases by approximately 39 times. The latter is associated with the lengthening of the field envelope. Accordingly, in the process of amplification, the emission spectrum is narrowed.

Similarly to the case of ellipticity-increasing amplification, the energy of ASE is insignificant (however, ASE manifests itself in a distortion of the ellipticity space-time dependence at the front edge of the amplified HH signal, $\tau \leq 50$ fs). Thus, the proposed approach makes it possible to boost the energy and peak intensity of circularly polarized resonant radiation by tens of times at the cost of the ellipticity decrease by approximately 4% (the ellipticity is less reduced at the leading edge of the XUV pulse and decreases more at its trailing edge).

V. NUMERICAL RESULTS FOR THE AMPLIFICATION OF A SET OF ELLIPTICALLY OR CIRCULARLY POLARIZED HIGH-ORDER HARMONICS

Next, we will consider the amplification of a set of five elliptically or circularly polarized high-order harmonics forming a train of approximately 1 fs pulses. We will assume that at the entrance to the medium, each of the harmonics is characterized by an envelope of the form (11), while the initial phases, amplitudes, and polarization states of all harmonics are the same.

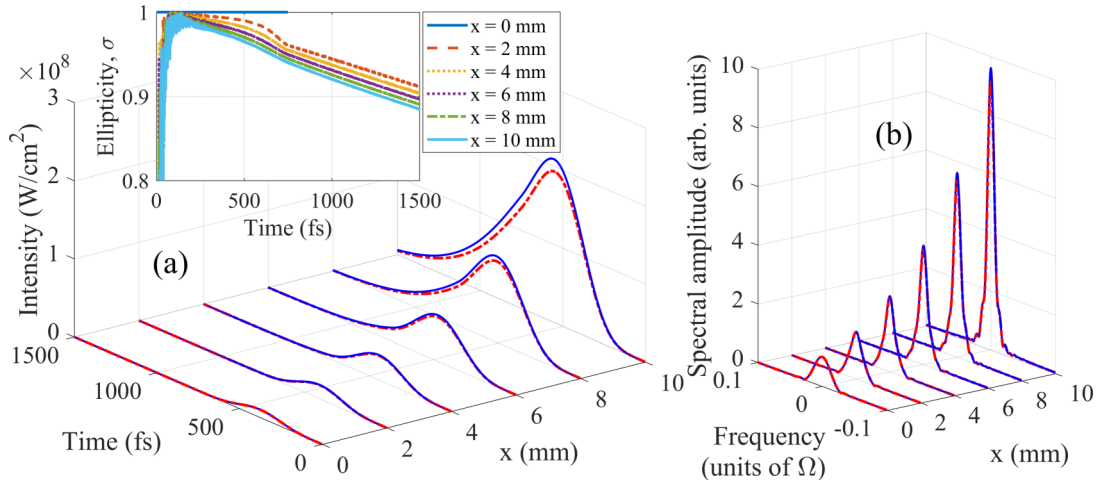


FIG. 7. (a) Dependences of the intensities of the polarization components of the XUV field on the local time, τ , corresponding to Fig. 6, at different lengths of the medium: $x = 0$ mm (incident field), 2 mm, 4 mm, 6 mm, 8 mm, and 10 mm. Red dash-dotted curve corresponds to the y -polarization component of the field, while blue solid curve shows the z component. The inset shows the time dependences of ellipticity of the field at the same lengths of the medium (with increasing medium length, the ellipticity decreases). The drop of ellipticity at $\tau \leq 50$ fs is caused by the ASE of the medium. (b) Spectral amplitudes of the polarization components of the XUV field at the same propagation distances through the medium. Red dash-dotted curve and lower gain correspond to the y component of the field; blue solid curve and higher gain correspond to the z component. The curves largely overlap at all the lengths of the medium and are normalized to the peak amplitude of the Fourier transform of the y component of the seeding radiation.

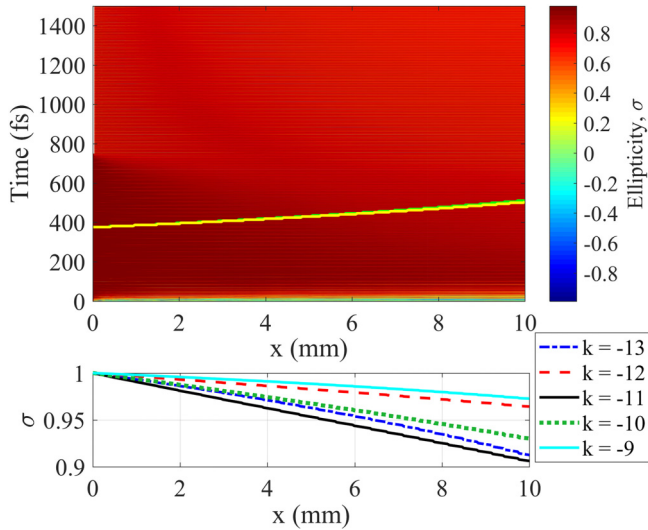


FIG. 8. Top panel: Space-time dependence of the ellipticity, σ , of the set of the 107th, 109th, 111th, 113th, and 115th harmonics of the modulating field ($k = -13, -12, -11, -10$, and -9 , respectively). The incident radiation is circularly polarized, $\sigma(x = 0) = 1$. Largely overlapping green and yellow curves show the positions of the maxima of the envelopes of the z - and y -polarization components of the field, respectively. Bottom panel: Ellipticity of each individual harmonic (harmonics are numbered by the index k) at the maximum of the total intensity of all harmonics as a function of the length of the medium, x .

A. Polarization-maintaining amplification of a set of high harmonics

First, we will consider the amplification of a train of circularly polarized pulses ($\sigma = 1$ at $x = 0$) formed by a combination of 107th, 109th, 111th, 113th, and 115th harmonics of the modulating field ($k = -13, -12, -11, -10$, and -9 , respectively). The pulse duration at the entrance to the medium is 0.9 fs, the pulse repetition period is 5.3 fs, the central wavelength is 29.18 nm, and the peak intensity of each of the y - and z -polarization components of the harmonic field is 5×10^7 W/cm². It is worth noting that we consider the shortest wavelength of the modulating field, at which the amplification of elliptically or circularly polarized high harmonics is possible in a neonlike Ti¹²⁺ active medium. Accordingly, 0.9 fs is the minimum duration of elliptically or circularly XUV radiation pulse which can be amplified while maintaining ellipticity.

The space-time dependence of the ellipticity of the amplified radiation, as well as the position of the maximum of its intensity envelope (the envelopes of the polarization components almost coincide on the scale of the figure), are shown in the top panel in Fig. 8. The bottom panel of Fig. 8 shows the spatial dependences of the ellipticity of each of the harmonics separately at the time instant corresponding to the maximum of the intensity envelope of the total harmonic field (which itself depends on the propagation distance, see the yellow curve on the top panel of Fig. 8). As seen from Fig. 8, the ellipticity of harmonics of different orders decreases at different rates, which are determined by the differences between the gain factors for the y and z components of the field of each harmonic; see Fig. 3.

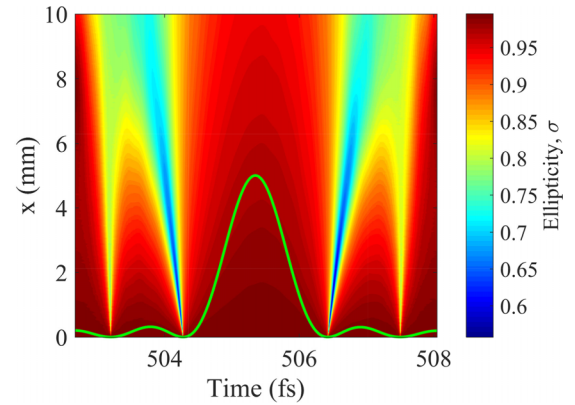


FIG. 9. Enlarged view of the fragment of the top panel of Fig. 8 corresponding to the time interval $502.7 \text{ fs} \leq \tau \leq 508 \text{ fs}$ equal in duration to the half-cycle of the modulating field. The vertical and horizontal axes are reversed. Green curve shows the shape of the pulses of the amplified radiation (time dependence of the intensity) at the entrance to the medium, $x = 0$.

In general, Fig. 8 resembles Fig. 6; however, in contrast to the latter, in Fig. 8, a small-scale structure appears due to a change in the contribution of each of the harmonics to the resulting field on a timescale of a fraction of the IR field cycle. This structure in the function $\sigma(x, \tau)$ is shown in Fig. 9, which is plotted for a time interval equal to a half-cycle of the modulating field and located in the region of the maximum of the amplified radiation envelope at $x = 10$ mm. For clarity, Fig. 9 also shows the time dependence of the intensity of the seed radiation (the evolution of the pulse shape with increasing length of the medium is illustrated in Fig. 10(a)). As follows from Fig. 9, at the moments of time corresponding to the constructive interference of harmonics and the formation of a burst in the intensity of the resulting field, the ellipticity also reaches its maximum, which is $\sigma \approx 0.95$ at $x = 10$ mm. The ellipticity decreases significantly only where harmonics of different orders are in antiphase with each other, and the resulting field is close to zero. The main features of the small-scale structure of the function $\sigma(x, \tau)$ shown in Fig. 9 are repeated on every half-cycle of the modulating field in the most energetic part of the pulse train.

In Fig. 10 we show the local time dependences of intensity [Fig. 10(a)] and ellipticity [Fig. 10(b)] of the XUV radiation within the same sub-IR-field-cycle time interval at a few propagation distances through the medium. As follows from Fig. 10(a), with increasing propagation distance the pulse duration increases from 0.9 fs to 1.3 fs because of nonuniform amplification of the harmonics of different orders [see Fig. 11(b)], while the peak ellipticity decreases from 1 to 0.95 because of a slightly stronger amplification of z -polarization component of the HH field compared to the y -polarization; see Fig. 11(a). The appearance of the dips in the ellipticity time dependence in Fig. 10(b) is caused by the difference in the timing of the minima of the z - and y -polarization components of the field, which, in turn, originates from the difference in the spectral composition of the polarization components; see Fig. 11(b).

In Fig. 11 we plot the picosecond-scale local time dependences of the intensities [Fig. 11(a)] and the amplitude spectra

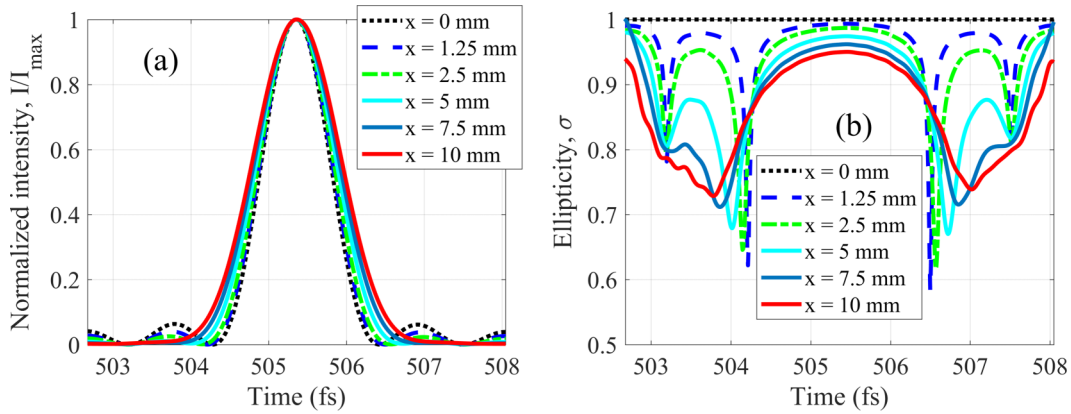


FIG. 10. (a) Local time dependence of the total intensity of the amplified XUV radiation corresponding to Fig. 9 within a half-cycle of the IR field at different lengths of the medium: $x = 0$ mm (incident field), 1.25 mm, 2.5 mm, 5 mm, 7.5 mm, and 10 mm. The time interval is chosen at the peak of the envelope of the total intensity at $x = 10$ mm; see Fig. 12. With increasing length of the medium, the pulse duration grows from $\tau_{\text{pulse}} = 0.9$ fs at $x = 0$ mm to $\tau_{\text{pulse}} = 1.3$ fs at $x = 10$ mm. (b) Corresponding variation of ellipticity of the XUV field within an IR field half-cycle. With increasing medium length, the peak ellipticity decreases from $\sigma = 1$ at $x = 0$ mm to $\sigma = 0.95$ at $x = 10$ mm.

[Fig. 11 (b)] of the polarization components of the XUV radiation at different lengths of the medium. Figure 11(a) generally resembles Fig. 7(a), which corresponds to the polarization-maintaining amplification of a single harmonic [the rapid intensity oscillations in Fig. 11(a), caused by the interference of the harmonics of different orders, are not resolved within the scale of the figure, and merge in a shaded area]. In turn, the output radiation spectra in Fig. 11(b) generally follow the gain spectrum of the active medium shown in Fig. 3: the 11th and 13th harmonics corresponding to $k = -11$ and $k = -10$ are amplified most efficiently, while the rest of the harmonics are amplified to a lesser degree, which results in reduction of the effective width of the harmonic emission spectrum with increasing propagation distance. Similar to Fig. 7(b), the emission spectrum of each individual harmonic narrows and the duration of its envelope increases, which

leads to an increase in the duration of the resulting pulse train in Fig. 11(a). Furthermore, the spectral composition of the radiation varies with time: in the vicinity of the maximum of the intensity envelope, harmonics of different orders have comparable amplitudes, while in the tail of the envelope, the 11th and 13th harmonics, which experienced the greatest amplification, dominate.

Figure 12 illustrates the results of amplification of the HH field in a 10 mm long active medium. Figure 12(a) shows the picosecond scale time dependencies of intensity and the ellipticity envelope (which is the ellipticity at the maxima of the individual pulses) of the total harmonic field, superimposed on each other, while in Fig. 12(b) we plot the time dependencies of intensity and ellipticity within an IR field half-cycle at the peak of the intensity envelope in Fig. 12(a). As follows from Fig. 12(a), at a medium length of 10 mm, the peak total

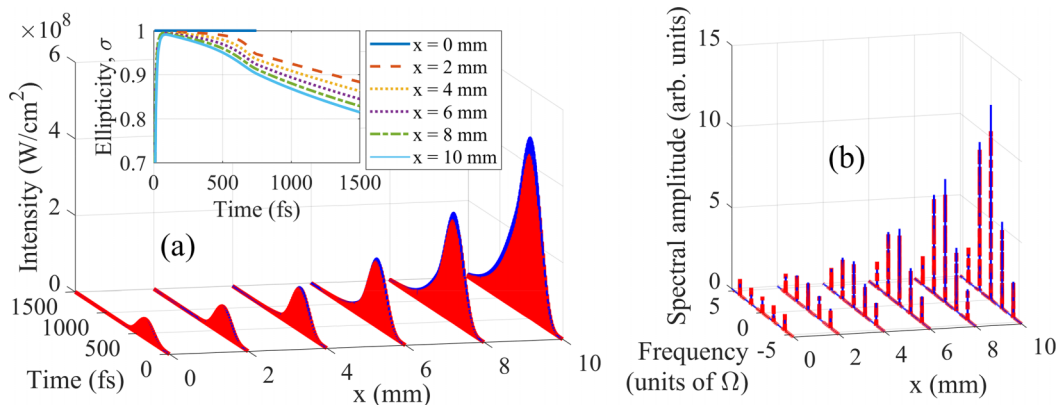


FIG. 11. (a) Dependences of the intensities of the polarization components of the XUV field on the local time, τ , corresponding to Fig. 8, at different lengths of the medium: $x = 0$ mm (incident field), 2 mm, 4 mm, 6 mm, 8 mm, and 10 mm. Red (light gray) curve corresponds to the y -polarization component of the field, while blue (dark gray) curve shows the z component. The inset shows the time dependencies of the ellipticity envelope of the field (the ellipticity at the maxima of the individual pulses) at the same lengths of the medium (with increasing medium length, the ellipticity decreases). The drop of ellipticity at $\tau \leq 50$ fs is caused by the ASE. (b) Spectral amplitudes of the polarization components of the XUV field at the same propagation distances in the medium. Red dash-dotted curve and lower gain correspond to the y component of the field; blue thin solid curve and higher gain correspond to the z component. The curves largely overlap at all the lengths of the medium and are normalized to the peak amplitude of the Fourier transform of the y component of the seeding radiation.

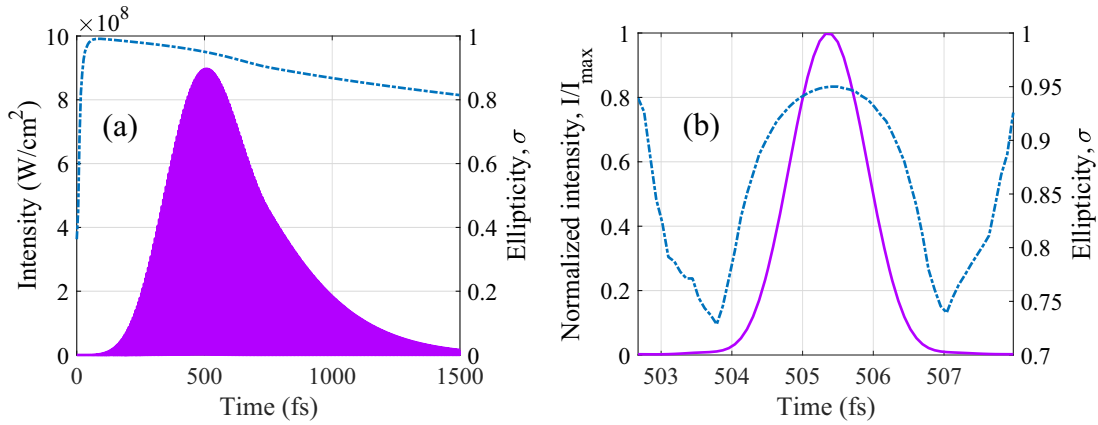


FIG. 12. (a) Local time dependences of the total intensity (solid lavender curve, left vertical axis) and the ellipticity envelope (see the text; dash-dotted blue curve, right vertical axis) of the XUV pulse train, corresponding to Figs. 8–11, amplified in 10 mm thick medium. (b) Same as in (a), but within a single half-cycle of the IR field at the maximum of the intensity envelope (in this case, the dash-dotted blue curve shows the instantaneous value of the ellipticity). The XUV intensity in (b) is normalized to its peak value, $I_{\text{max}} = 8.9 \times 10^8$ W/cm^2 .

intensity of the radiation increases by 8.9 times (to a value of about 8.9×10^8 W/cm^2), and due to an increase in the duration of the polarization components of the field, as well as an increase in the duration of each of the pulses in the train, the radiation energy increases by 22.1 times. At the maximum of the intensity envelope (at $x = 10$ mm and $\tau = 505.3$ fs), the ellipticity of the amplified radiation is 0.95. According to Fig. 12(b), the ellipticity does not change considerably within the pulse duration.

Thus, using a modulated active medium of a plasma-based x-ray laser, it is possible to increase the energy of XUV pulses of circularly polarized radiation by more than an order of magnitude without significantly changing their polarization state.

B. Ellipticity-increasing amplification of a set of high harmonics

Finally, we will consider the possibility of increasing the ellipticity of the train of sub-fs pulses in the process of their amplification using the example when such a train is formed by a combination of the 127th, 131st, 135th, 139th, and 143rd harmonics of the modulating field ($k = -3, -1, 1, 3, \text{ and } 5$; see Fig. 3). In this case, the pulse duration at the entrance to the medium is 450 as, the pulse repetition period is 2.69 fs, and the central wavelength is 23.97 nm. The peak intensity of the y component of the total harmonic field at $x = 0$ is 5×10^7 W/cm^2 . We take the peak intensity of the z component of the field to be 1.65×10^8 W/cm^2 , and the ellipticity of the field at the entrance to the medium is $\sigma(x = 0, \tau) = 0.55$.

The change of ellipticity due to the predominant amplification of the y component of the field as it propagates in the medium is shown in Figs. 13 and 14. Figure 13 is drawn for a time interval exceeding the duration of the envelope of the amplified radiation, while in Fig. 14, the dependence $\sigma(x, \tau)$ is shown for the half-cycle of the modulating field in the vicinity of the maximum of the radiation envelope at $x = 11.56$ mm (which is the optimal propagation distance, see the discussion below). The top panel of Fig. 13 also depicts the spatial dependences of the time instants at which the maximum of the harmonic intensity envelope is reached for each of the

polarization components of the XUV field and for their sum. The bottom panel of Fig. 13 shows the spatial dependences of the ellipticity of each harmonic separately at the maximum of the envelope of the total harmonic field (the sum over the polarizations). In general, Fig. 13 is similar to Fig. 4 demonstrating the ellipticity-increasing amplification of a single harmonic. With an increase of the length of the medium, the maximum of harmonic ellipticity shifts from $\tau \approx 750$ fs to earlier moments of local time, while the maximum of the

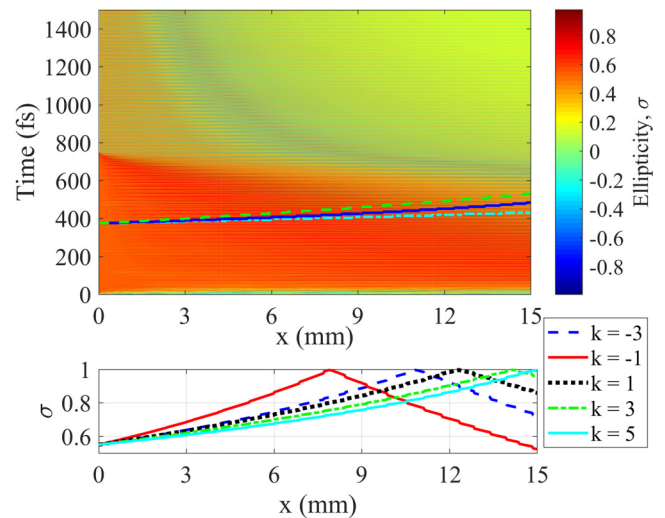


FIG. 13. Top panel: Space-time dependence of ellipticity, σ , of the set of the 127th, 131st, 135th, 139th, and 143rd harmonics of the modulating field ($k = -3, -1, 1, 3, \text{ and } 5$, respectively). At the entrance to the medium, $\sigma(x = 0) = 0.55$ (z polarization dominates). Cyan dash-dotted and green dashed curves show the positions of the maxima of the envelopes of the z- and y-polarized components of the total harmonic field. Blue solid curve shows the maximum of the total intensity of both polarization components. Bottom panel: Ellipticity of each individual harmonic (harmonics are numbered by the index k) at the maximum of the total intensity (summed over all harmonics and both polarization components) as a function of the medium length, x .

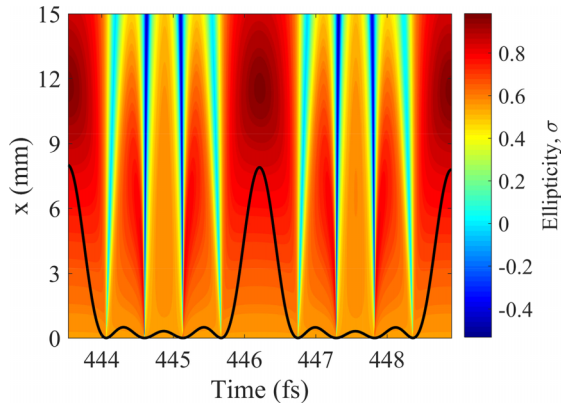


FIG. 14. Enlarged view of the fragment of the top panel of Fig. 13 corresponding to the time interval $443.5 \text{ fs} \leq \tau \leq 448.9 \text{ fs}$. The vertical and horizontal axes are reversed. Black curve shows the shape of the pulses of the amplified radiation (time dependence of the intensity) at the entrance to the medium, $x = 0$.

intensity envelope, on the contrary, shifts from $\tau = 375 \text{ fs}$ to later times. In the vicinity of $x = 11.56 \text{ mm}$, these maxima coincide at $\tau \approx 446.2 \text{ fs}$; in this case, at the maximum of the total intensity of the polarization components, the harmonic field acquires almost circular polarization, $\sigma = 0.998$.

At the same time, similar to the case of polarization-maintaining amplification of five harmonics shown in Fig. 8, a small-scale structure appears in the space-time dependence of the harmonic ellipticity, due to (a) the difference in the ellipticity of the harmonics of different orders and (b) a change in the conditions of their interference on a time scale of a fraction of the IR field cycle. This structure in the function $\sigma(x, \tau)$ is shown in Fig. 14. Similar to Fig. 9, the ellipticity maximum of the XUV radiation coincides with the maximum of its intensity, while where the intensity of the total radiation of harmonics is close to zero, a decrease of ellipticity is observed.

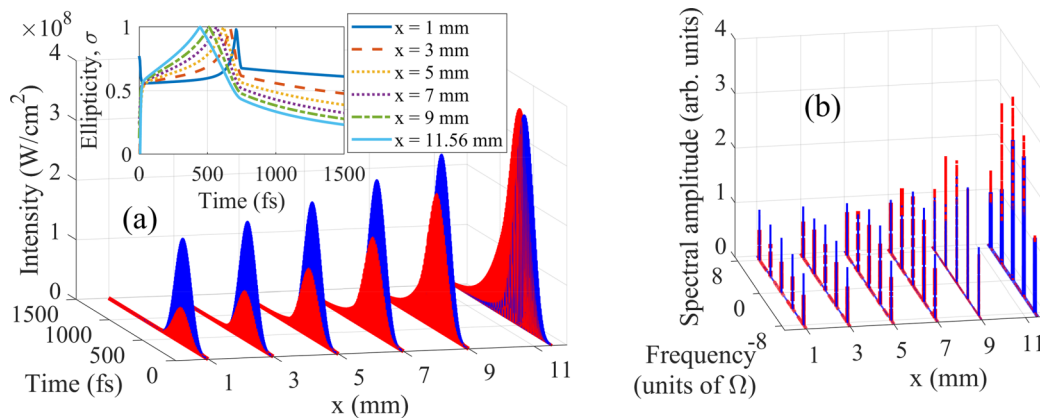


FIG. 15. (a) Dependences of the intensities of the polarization components of the XUV field on the local time, τ , corresponding to Fig. 13, at different lengths of the medium: $x = 1 \text{ mm}$, 3 mm , 5 mm , 7 mm , 9 mm , and 11.56 mm . Red (light gray) curve corresponds to the y -polarization component of the field, while blue (dark gray) curve shows the z component. The inset shows the time dependences of the ellipticity envelope of the field at the same lengths of the medium (for a larger length, the peak of ellipticity shifts to an earlier time). The change in the ellipticity at the very initial times is caused by the ASE. (b) Spectral amplitudes of the polarization components of the XUV field at the same propagation distances in the medium. Red dash-dotted curve and higher gain correspond to the y component of the field; blue thin solid curve and lower gain correspond to the z component. The curves are normalized to the peak amplitude of the Fourier transform of the z component of the seeding radiation.

The time dependences of the intensities of the polarization components of the amplified radiation and the corresponding spectra at different lengths of the medium are shown in Fig. 15(a) and Fig. 15(b), respectively [the individual sub-fs pulses are not resolved in Fig. 15(a) and merge in a shaded area]. Just as in the case of ellipticity-increasing amplification of a single harmonic (see Fig. 5), the polarization component experiencing the greatest amplification in the medium (in this case, y component) is stretched in time. At the same time, similar to the case of amplification of the set of five harmonics with approximate maintaining of their polarization (see Fig. 11), as a result of the predominant amplification of the 131st, 135th, and 139th harmonics of the modulating field, the effective width of the radiation spectrum decreases during amplification. It leads to lengthening of the pulses from 450 as to 600 as in the vicinity of the maximum of the intensity envelope; see Fig. 16(a), where the evolution of the pulse shape is traced with an increase of the propagation distance. The corresponding evolution of the sub-IR-field-cycle time dependence of ellipticity is shown in Fig. 16(b), which represents the cuts of Fig. 14 for a few fixed propagation distances.

Figure 17 plots the superimposed time dependencies of the total intensity (summed over the polarization components) and ellipticity of the amplified XUV field at the optimal length of the medium, $x = 11.56 \text{ mm}$, on the picosecond [Fig. 17(a)] and a sub-IR-field-cycle [Fig. 17(b)] timescales. In Fig. 17(a) and Fig. 17(b) we plot the ellipticity envelope (the ellipticity at the maxima of individual sub-fs pulses) and the instantaneous ellipticity of the total harmonic field, respectively. As can be seen from Fig. 17(a), the increase in ellipticity is accompanied by 5.1 times increasing energy of the XUV field. In turn, as follows from Fig. 17(b), the ellipticity of the HH field shows just a moderate variation within the pulse duration. Thus, the proposed method makes it possible to change the polarization of the train of sub-fs XUV pulses from elliptical to nearly circular with a simultaneous increase in their energy by several times.

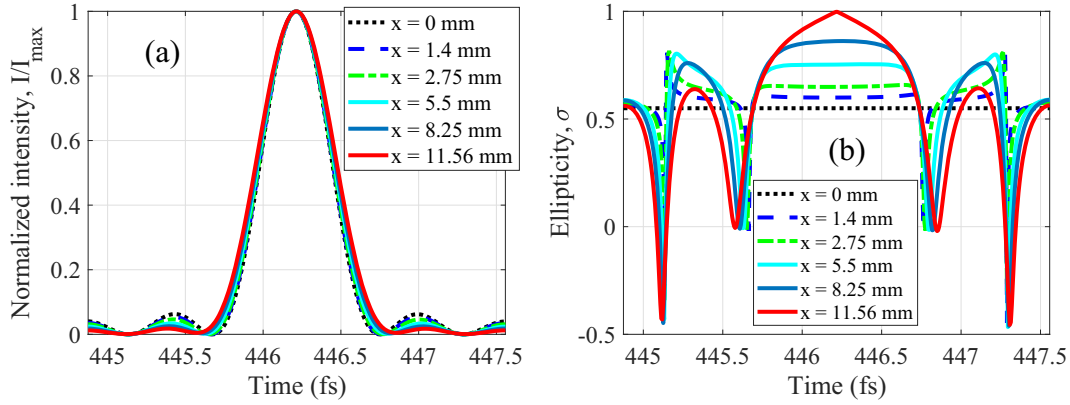


FIG. 16. (a) The shape of individual pulses from the pulse train shown in Fig. 15 at different lengths of the medium: $x = 0$ mm (incident field), 1.4 mm, 2.75 mm, 5.5 mm, 8.25 mm, and 11.56 mm. The vertical and horizontal axes show the total intensity of the polarization components of the XUV field and the local time, τ , respectively. The time interval corresponds to the peak of the envelope of the total intensity at $x = 11.56$ mm. With increasing length of the medium, the pulse duration grows from $\tau_{\text{pulse}} = 450$ as at $x = 0$ mm to $\tau_{\text{pulse}} = 600$ as at $x = 11.56$ mm. (b) Variation of ellipticity of the XUV field, corresponding to (a), within an IR field quarter-cycle. With increasing medium length, the peak ellipticity increases from $\sigma = 0.55$ at $x = 0$ mm to $\sigma = 0.998$ at $x = 11.56$ mm.

VI. CONCLUSION

In this paper, we presented the detailed analytical and numerical study of the HH amplification process in an active medium of neonlike x-ray laser dressed by a replica of an IR field used for HH generation. We derived an analytical solution describing evolution of an individual harmonic detuned from resonance by an even multiple of the modulating field frequency during its propagation through an active medium, caused by the interaction of each of the orthogonal polarization components of the HH field with the corresponding induced gain line of the active medium. On the basis of the derived solution we have shown the possibility to amplify a single HH with (a) preservation, (b) increase, or (c) decrease in the harmonic ellipticity depending on (i) the detuning of the harmonic frequency from the time-averaged frequency of the inverted transition in the presence of the IR field and (ii) the orientation of the main axis of the harmonic polarization

ellipse with respect to the polarization of the IR field. It is shown that the frequencies of the induced gain lines can be consistently tuned in a wide range by a coordinated change in the intensity and wavelength of the modulating field. This opens the possibility to tune the proper induced gain lines (a separate line for each of the orthogonal polarization components of the HH field) in resonance with the desired high-order harmonic and, thus, to control the harmonic polarization state by changing the relative amplitudes of its polarization components, which is impossible in the absence of the modulation.

We numerically analyzed the spectral, temporal, and polarization properties of an individual elliptically or circularly polarized HH as it passes through a neonlike Ti^{12+} active medium modulated by the IR field with a wavelength of $3.2 \mu\text{m}$. For the considered active medium this is the minimum wavelength of the modulating field, at which both polarization components of the HH field can be jointly amplified, which also corresponds to the broadest spectral distribution of the

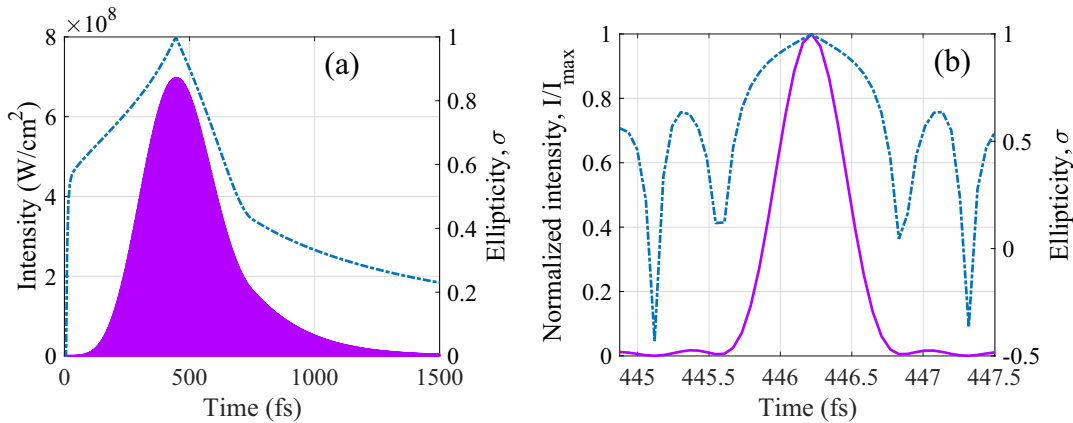


FIG. 17. (a) Local time dependences of the total intensity (solid lavender curve, left vertical axis) and the ellipticity envelope (dash-dotted blue curve, right vertical axis) of the XUV pulse train, corresponding to Figs. 13–16, amplified in 11.56 mm long medium. (b) Same as in (a), but within a single quarter-cycle of the IR field at the maximum of the intensity envelope (in this case, the dash-dotted blue curve shows the instantaneous value of the ellipticity). The XUV intensity in (b) is normalized to its peak value, $I_{\max} = 6.96 \times 10^8 \text{ W/cm}^2$.

medium gain. The two specific cases were considered: (a) the 153rd harmonic of the modulating field ($\lambda_{H153} = 21.14$ nm) with an ellipticity of 0.3, which is amplified with ellipticity enhancement, and (b) the 113th harmonic of the modulating field ($\lambda_{H113} = 28.66$ nm) with circular polarization, which is amplified with approximate polarization maintenance. It is shown that in both cases the polarization component of the HH field, which experiences the stronger amplification, is spectrally narrowed and lengthened in time, which results in time variation of ellipticity of the amplified radiation. This time variation is rather moderate in the case of the polarization maintaining amplification and much more substantial for the amplification with an ellipticity enhancement (however, in the latter case, at the optimal length of the medium, the maxima of radiation intensity and ellipticity coincide). In particular, for the Ti^{12+} active plasma medium with the unperturbed intensity gain 70 cm^{-1} we have shown that the radiation of the 153rd harmonic of the modulating field acquires circular polarization at the maximum of the envelope of the total intensity of its polarization components with medium length 6.1 mm. The change in the polarization state of the harmonic in this case is accompanied by an increase in energy of its most amplified polarization component. It is also shown that the peak intensity of the radiation of the circularly polarized 113th harmonic of the modulating field can be increased by a factor of 20 with an increase in its energy by a factor of 39 (due to the lengthening of the radiation envelope) in a 10 mm long modulated medium at the cost of an ellipticity decrease by 4%.

Furthermore, we extended the results obtained in [32] complementing them with the numerical studies of the spatial-temporal dependence of ellipticity of a set of harmonics, composing a train of sub-fs pulses with the minimum possible pulse duration for the considered active plasma medium. We have shown that because of the difference in the gain coefficients for the harmonics of different orders, at the output from an optically deep active medium some of the harmonics dominate over the others due to stronger amplification, which results in narrowing of the total harmonic spectrum and an increase in the duration of each femto- or sub-fs pulse. In addition, the difference in both the amplitudes and the polarization states of harmonics of different orders, caused by slightly different conditions of their amplification, results in the variation of ellipticity of the XUV radiation within a half-cycle of the fundamental frequency IR field. However, in the most energetic part of the pulse train, the ellipticity reaches the maximum value at the moments of time corresponding to the formation of a burst in the resulting field of harmonics, and decreases significantly only where the harmonics of different

orders are in antiphase with each other, and the resulting field is close to zero. Accordingly, only a moderate variation of ellipticity occurs within the duration of each of the amplified pulses.

The discussed method can be extended to other neonlike and nickellike (in particular, Mo^{14+} or Ag^{19+}) ions due to the similarity of the energy structure. In prospect, this opens up the possibility of more flexible control over the position of the induced gain lines and, in particular, the possibility to amplify the harmonic emission of elliptical or circular polarization in shorter-wavelength spectral ranges. All in all, this approach might allow for a considerable increase in both the energy and ellipticity of a single high harmonic as well as of a few femtosecond or sub-fs XUV radiation pulses, which can be used for probing chiral and magnetic media.

ACKNOWLEDGMENTS

V.A.A., I.R.Kh., and M.Yu.R. acknowledge funding from the Ministry of Science and Higher Education of the Russian Federation (state assignment for the Institute of Applied Physics RAS, Project No. 0030-2021-0012). O.K. appreciates support by the National Science Foundation (Grant No. PHY-2012194).

APPENDIX A

Let us choose the z axis as the quantization axis. In this case, the dipole moment of the transition from the state $|1\rangle$ to the state $|2\rangle$ of Ti^{12+} ions [see Fig. 1(a)] will be oriented along the z axis, while the dipole moments of the transitions between the states $|1\rangle$ and $|3\rangle$, as well as between the states $|1\rangle$ and $|4\rangle$, will have components along the x and y axes:

$$\begin{aligned}\vec{d}_{21} &= \vec{z}_0 d_z, \\ \vec{d}_{31} &= -\vec{x}_0 d_x - i\vec{y}_0 d_y, \\ \vec{d}_{41} &= \vec{x}_0 d_x - i\vec{y}_0 d_y,\end{aligned}\quad (A1)$$

where \vec{x}_0 , \vec{y}_0 , and \vec{z}_0 are unit vectors along the x , y , and z axes, respectively; $d_z = D/\sqrt{3}$ and $d_x = d_y = D/\sqrt{6}$, whereas $D \equiv |(3p^1S_0||D||3s^1P_1)|$ is the reduced matrix element of the transition dipole moment (see [60]), which, according to [61], can be calculated through the spontaneous emission rate at the inverted transition, $W(3p^1S_0; 3s^1P_1)$, as $D = \sqrt{\frac{3\hbar c^3}{4\omega^3} W(3p^1S_0; 3s^1P_1)}$.

The evolution of the quantum state of Ti^{12+} ions under the influence of XUV radiation (1) is described by the equations for the density matrix elements ρ_{ij} (von Neumann equations with relaxation):

$$\begin{aligned}\frac{\partial \rho_{11}}{\partial t} + \gamma_{11}\rho_{11} &= \frac{i}{\hbar} \sum_{s=1}^4 (\rho_{s1}\vec{d}_{1s} - \rho_{1s}\vec{d}_{s1})\vec{E}, \\ \frac{\partial \rho_{ii}}{\partial t} + \gamma_{ii}\rho_{ii} &= A\rho_{11} + \frac{i}{\hbar} \sum_{s=1}^4 (\rho_{si}\vec{d}_{is} - \rho_{is}\vec{d}_{si})\vec{E}, \quad \text{if } i \neq 1, \\ \frac{\partial \rho_{ij}}{\partial t} + [i\omega_{ij}(t, x) + \gamma_{ij}]\rho_{ij} &= \frac{i}{\hbar} \sum_{s=1}^4 (\rho_{sj}\vec{d}_{is} - \rho_{is}\vec{d}_{sj})\vec{E}, \quad \text{if } j \neq i,\end{aligned}\quad (A2)$$

where $\vec{E} = \vec{E}(x, t)$ is the XUV radiation in the medium, $\omega_{ij}(t, x)$ are the frequencies of quantum transitions determined by Eqs. (4), A is the rate of spontaneous radiative transition from the $|1\rangle$ state to each of the $|2\rangle$, $|3\rangle$, and $|4\rangle$ states, $1/A = 242.5$ ps [48], and γ_{ij} are the relaxation rates of the density-matrix elements, which are determined as follows. The relaxation rate of the density matrix diagonal element ρ_{ii} is the sum of the rates of radiative transitions from the $|i\rangle$ state to all lower-energy ionic states, $\Gamma_{\text{rad}}^{(i)}$, and the rate of tunneling ionization from the $|i\rangle$ state under the influence of the IR field, $w_{\text{ion}}^{(i)}$ (which is calculated using the Perelomov-Popov-Terent'ev formula [50]), i.e., $\gamma_{ii} = \Gamma_{\text{rad}}^{(i)} +$

$w_{\text{ion}}^{(i)}$. In the considered case of Ti^{12+} ions $1/\Gamma_{\text{rad}}^{(1)} \approx 50.2$ ps and $1/\Gamma_{\text{rad}}^{(2,3,4)} \approx 3.34$ ps, while in the range of IR intensities under consideration, ionization from resonant states is not significant, $w_{\text{ion}}^{(i)} < \Gamma_{\text{rad}}^{(i)}$ ($\forall i$). The relaxation rate of an off-diagonal element ρ_{ij} of the density matrix is determined as $\gamma_{ij} = (\gamma_{ii} + \gamma_{jj})/2 + \gamma_{\text{Coll}}$, where γ_{Coll} is the frequency of collisions in the plasma.

Next, we turn to local time $t \rightarrow \tau = t - x\sqrt{\varepsilon_{\text{pl}}^{(XUV)}}/c$ and look for a solution of the system of equations (A2) using the approximation of slowly varying amplitudes, i.e., assuming that

$$\begin{aligned} \vec{E}(x, \tau) &= \frac{1}{2}[\vec{z}_0\vec{E}_z(x, \tau) + \vec{y}_0\vec{E}_y(x, \tau)] \exp(-i\omega\tau) + \text{c.c.}, \\ \rho_{12}(x, \tau) &= \tilde{\rho}_{12}(x, \tau)e^{-i\omega\tau}, \quad \rho_{13}(x, \tau) = \tilde{\rho}_{13}(x, \tau)e^{-i\omega\tau}, \quad \rho_{14}(x, \tau) = \tilde{\rho}_{14}(x, \tau)e^{-i\omega\tau}, \\ \rho_{ij} &= \rho_{ji}^* \text{ and } \rho_{ij}(x, \tau) = \tilde{\rho}_{ij}(x, \tau) \text{ if } ij \neq \{12, 21, 13, 31, 14, 41\}, \end{aligned} \quad (\text{A3})$$

where $\vec{E}_z(x, \tau)$ and $\vec{E}_y(x, \tau)$ are slowly varying complex amplitudes of the polarization components of the XUV radiation in the medium, $|\frac{\partial \vec{E}_{z,y}}{\partial \tau}| \ll \omega|\vec{E}_{z,y}|$ and $|\frac{\partial \vec{E}_{z,y}}{\partial x}| \ll \frac{\omega\sqrt{\varepsilon_{\text{pl}}^{(XUV)}}}{c}|\vec{E}_{z,y}|$, whereas $\tilde{\rho}_{ij}(x, \tau)$ are slowly varying amplitudes of the density-matrix elements of the medium, $|\frac{\partial \tilde{\rho}_{ij}}{\partial \tau}| \ll \omega|\tilde{\rho}_{ij}|$ and $|\frac{\partial \tilde{\rho}_{ij}}{\partial x}| \ll \frac{\omega\sqrt{\varepsilon_{\text{pl}}^{(XUV)}}}{c}|\tilde{\rho}_{ij}|$. Assuming that the radiation frequency of (1) is close to the transition frequencies $|1\rangle \leftrightarrow |2\rangle$ and $|1\rangle \leftrightarrow |3\rangle, |4\rangle$, the displacement of which under the influence of the IR field is taken into account, and using the rotating wave approximation, the system of Eqs. (A2) can be represented as

$$\begin{aligned} \frac{\partial \tilde{\rho}_{11}}{\partial \tau} + \gamma_{11}\tilde{\rho}_{11} &= \frac{i}{2\hbar}d_z(\tilde{\rho}_{12}^*\vec{E}_z - \tilde{\rho}_{12}\vec{E}_z^*) - \frac{1}{2\hbar}d_y(\tilde{\rho}_{13}^*\vec{E}_y + \tilde{\rho}_{13}\vec{E}_y^*) - \frac{1}{2\hbar}d_y(\tilde{\rho}_{14}^*\vec{E}_y + \tilde{\rho}_{14}\vec{E}_y^*), \\ \frac{\partial \tilde{\rho}_{22}}{\partial \tau} + \gamma_{22}\tilde{\rho}_{22} &= A\tilde{\rho}_{11} - \frac{i}{2\hbar}d_z(\tilde{\rho}_{12}^*\vec{E}_z - \tilde{\rho}_{12}\vec{E}_z^*), \\ \frac{\partial \tilde{\rho}_{33}}{\partial \tau} + \gamma_{33}\tilde{\rho}_{33} &= A\tilde{\rho}_{11} + \frac{1}{2\hbar}d_y(\tilde{\rho}_{13}^*\vec{E}_y + \tilde{\rho}_{13}\vec{E}_y^*), \\ \frac{\partial \tilde{\rho}_{44}}{\partial \tau} + \gamma_{44}\tilde{\rho}_{44} &= A\tilde{\rho}_{11} + \frac{1}{2\hbar}d_y(\tilde{\rho}_{14}^*\vec{E}_y + \tilde{\rho}_{14}\vec{E}_y^*), \\ \frac{\partial \tilde{\rho}_{12}}{\partial \tau} + [i(\omega_{12}(\tau, x) - \omega) + \gamma_{12}]\tilde{\rho}_{12} &= -\frac{i}{2\hbar}d_z(\tilde{\rho}_{11} - \tilde{\rho}_{22})\vec{E}_z - \frac{1}{2\hbar}d_y\tilde{\rho}_{23}^*\vec{E}_y - \frac{1}{2\hbar}d_y\tilde{\rho}_{24}^*\vec{E}_y, \\ \frac{\partial \tilde{\rho}_{13}}{\partial \tau} + [i(\omega_{13}(\tau, x) - \omega) + \gamma_{13}]\tilde{\rho}_{13} &= \frac{1}{2\hbar}d_y(\tilde{\rho}_{11} - \tilde{\rho}_{33})\vec{E}_y + \frac{i}{2\hbar}d_z\tilde{\rho}_{23}\vec{E}_z - \frac{1}{2\hbar}d_y\tilde{\rho}_{34}^*\vec{E}_y, \\ \frac{\partial \tilde{\rho}_{14}}{\partial \tau} + [i(\omega_{14}(\tau, x) - \omega) + \gamma_{14}]\tilde{\rho}_{14} &= \frac{1}{2\hbar}d_y(\tilde{\rho}_{11} - \tilde{\rho}_{44})\vec{E}_y + \frac{i}{2\hbar}d_z\tilde{\rho}_{24}\vec{E}_z - \frac{1}{2\hbar}d_y\tilde{\rho}_{34}\vec{E}_y, \\ \frac{\partial \tilde{\rho}_{23}}{\partial \tau} + [i\omega_{23}(\tau, x) + \gamma_{23}]\tilde{\rho}_{23} &= \frac{i}{2\hbar}d_z\tilde{\rho}_{13}\vec{E}_z^* + \frac{1}{2\hbar}d_y\tilde{\rho}_{12}^*\vec{E}_y, \\ \frac{\partial \tilde{\rho}_{24}}{\partial \tau} + [i\omega_{24}(\tau, x) + \gamma_{24}]\tilde{\rho}_{24} &= \frac{i}{2\hbar}d_z\tilde{\rho}_{14}\vec{E}_z^* + \frac{1}{2\hbar}d_y\tilde{\rho}_{12}^*\vec{E}_y, \\ \frac{\partial \tilde{\rho}_{34}}{\partial \tau} + [i\omega_{34}(\tau, x) + \gamma_{34}]\tilde{\rho}_{34} &= \frac{1}{2\hbar}d_y\tilde{\rho}_{14}\vec{E}_y^* + \frac{1}{2\hbar}d_y\tilde{\rho}_{13}^*\vec{E}_y. \end{aligned} \quad (\text{A4})$$

In turn, when XUV radiation propagates in the active medium of a plasma-based x-ray laser, its slowly varying amplitude $\vec{E}(x, \tau) = \vec{z}_0\vec{E}_z(x, \tau) + \vec{y}_0\vec{E}_y(x, \tau)$ changes in accordance with the equation

$$\frac{\partial \vec{E}}{\partial x} = i2\pi \frac{\omega}{c\sqrt{\varepsilon_{\text{pl}}^{(XUV)}}} \vec{P}, \quad (\text{A5})$$

which is obtained from the wave equation after changing variables $x, t \rightarrow x, \tau$ within the approximation of slowly varying amplitudes [62]. In Eq. (A5), \vec{P} is the slowly varying amplitude of the resonant polarization of the medium $\vec{P}(x, \tau) = \frac{1}{2}\vec{P}(x, \tau) \exp(-i\omega\tau) + \text{c.c.}$, which is expressed through the density matrix in accordance with the equation

$$\vec{P} = N_{\text{ion}} \text{Tr}(\hat{d}\hat{\rho}) = N_{\text{ion}}(\rho_{12}\vec{d}_{21} + \rho_{13}\vec{d}_{31} + \rho_{14}\vec{d}_{41}) + \text{c.c.}, \quad (\text{A6})$$

where N_{ion} is the concentration of Ti^{12+} ions in the $|1\rangle$, $|2\rangle$, $|3\rangle$, and $|4\rangle$ states at the initial instant of time, whereas \hat{d} and $\hat{\rho}$ are the operators of dipole moment and density matrix of the medium, respectively. Using the explicit form (A1) of the dipole moments of the $|1\rangle \leftrightarrow |2\rangle$ and $|1\rangle \leftrightarrow |3\rangle$, $|4\rangle$ transitions, we can write the equations for the polarization components of the XUV field as follows:

$$\begin{aligned}\frac{\partial \tilde{E}_z}{\partial x} &= i4\pi N_{\text{ion}} d_z \frac{\omega}{c\sqrt{\varepsilon_{pl}^{(XUV)}}} \tilde{\rho}_{12}, \\ \frac{\partial \tilde{E}_y}{\partial x} &= 4\pi N_{\text{ion}} d_y \frac{\omega}{c\sqrt{\varepsilon_{pl}^{(XUV)}}} (\tilde{\rho}_{13} + \tilde{\rho}_{14}).\end{aligned}\quad (\text{A7})$$

Further, we will assume that at $\tau = t - x\sqrt{\varepsilon_{pl}^{(XUV)}}/c = 0$, among the states $|1\rangle - |4\rangle$, only the state $|1\rangle$ is populated: $\tilde{\rho}_{11}(x, \tau = 0) = 1$ and $\tilde{\rho}_{ii}(x, \tau = 0) = 0$ for $i \neq 1$. This approximation is justified by the fact that the rate of spontaneous radiative transitions from the state $|1\rangle$ to the lower-energy states is much lower than the rates of radiative transitions from the $|2\rangle$, $|3\rangle$, and $|4\rangle$ states, namely, $\Gamma_{\text{rad}}^{(1)} \ll \Gamma_{\text{rad}}^{(2,3,4)}$. As a result, during the evolution of a plasma created by a sequence of pump pulses that precede the pulses of both the resonant radiation (1) and the modulating field (2) and propagate along the x axis, the resonant Ti^{12+} ions accumulate in the state $|1\rangle$. Further, in order to simulate the amplified spontaneous emission (ASE) of the active medium, we set random initial

(at $\tau = 0$) values of coherences (off-diagonal elements of the density matrix) at the inverted $|1\rangle \leftrightarrow |2\rangle$, $|3\rangle$, $|4\rangle$ transitions (see [31,49,63]), whereas the initial values of the remaining coherences are equal to zero. We also note that at $\tau = 0$ the XUV radiation at the corresponding point in the medium (with the exception of the front boundary of the medium) is absent: $\tilde{E}_z(x \neq 0, \tau = 0) = 0$ and $\tilde{E}_y(x \neq 0, \tau = 0) = 0$.

Due to the absence of reflections of XUV radiation from the boundaries of the medium, the boundary conditions at the front side of the medium have the form $\tilde{E}_z(x = 0, \tau) = \tilde{E}_z^{(\text{inc})}(\tau)$ and $\tilde{E}_y(x = 0, \tau) = \tilde{E}_y^{(\text{inc})}(\tau)$. Similarly, at the back side of the medium ($x = L$), $\tilde{E}_z^{(\text{out})}(\tau) = \tilde{E}_z(x = L, \tau)$ and $\tilde{E}_y^{(\text{out})}(\tau) = \tilde{E}_y(x = L, \tau)$, where $\tilde{E}_z^{(\text{out})}$ and $\tilde{E}_y^{(\text{out})}$ are the polarization components of the slowly varying amplitude of the XUV radiation behind the medium, $\tilde{E}^{(\text{out})}(\tau) = \frac{1}{2}[\tilde{z}_0 \tilde{E}_z^{(\text{out})}(\tau) + \tilde{y}_0 \tilde{E}_y^{(\text{out})}(\tau)] \exp(-i\omega\tau) + \text{c.c.}$

Equations (A4) and (A7), together with the above-mentioned initial and boundary conditions, completely characterize the temporal dynamics and spatial evolution of resonant radiation and the quantum state of the active medium.

APPENDIX B

In the linear approximation, the amplification of the polarization components of the XUV radiation occurs independently, therefore, we consider them separately.

The z component of the XUV radiation in the medium satisfies the equations

$$\begin{aligned}\frac{\partial \tilde{E}_z}{\partial x} &= i4\pi N_{\text{ion}} d_z \frac{\omega}{c\sqrt{\varepsilon_{pl}^{(XUV)}}} \tilde{\rho}_{12}, \\ \frac{\partial \tilde{\rho}_{12}}{\partial \tau} + \{i(\bar{\omega}_{1r}^{(z)} - \omega) + i\Delta_{\Omega}^{(z)} \cos[2(\Omega\tau + \Delta Kx)] + \gamma_z\} \tilde{\rho}_{12} &= -in_{1r}^{(z)} \frac{d_z \tilde{E}_z}{2\hbar},\end{aligned}\quad (\text{B1})$$

where $\gamma_z \equiv \gamma_{12}$ and $n_{1r}^{(z)} = \tilde{\rho}_{11}(x, \tau) - \tilde{\rho}_{22}(x, \tau)$ is the population difference at the transition $|1\rangle \leftrightarrow |2\rangle$; in the approximation under consideration, $n_{1r}^{(z)} = 1$. Let's seek a solution for $\tilde{\rho}_{12}(x, \tau)$ in the form

$$\tilde{\rho}_{12}(x, \tau) = \hat{\rho}_{12}(x, \tau) \exp\{-iP_{\Omega}^{(z)} \sin[2(\Omega\tau + \Delta Kx)]\}, \quad (\text{B2})$$

where $P_{\Omega}^{(z)} = \frac{\Delta_{\Omega}^{(z)}}{2\Omega}$ is the frequency modulation index of the $|1\rangle \leftrightarrow |2\rangle$ transition under the influence of the IR field. The newly introduced function $\hat{\rho}_{12}(x, \tau)$ satisfies the equation

$$\begin{aligned}\frac{\partial \hat{\rho}_{12}}{\partial \tau} + [i(\bar{\omega}_{1r}^{(z)} - \omega) + \gamma_z] \hat{\rho}_{12} \\ = -i \frac{n_{1r}^{(z)} d_z}{2\hbar} \tilde{E}_z(x, \tau) \exp\{iP_{\Omega}^{(z)} \sin[2(\Omega\tau + \Delta Kx)]\}.\end{aligned}\quad (\text{B3})$$

In the following, we will seek solutions for $\hat{\rho}_{12}(x, \tau)$ and $\tilde{E}_z(x, \tau)$ in the form of the spectral decompositions:

$$\begin{aligned}\hat{\rho}_{12}(x, \tau) &= \int_{-\infty}^{\infty} \hat{\rho}_{12}^{(v)}(x, \nu) \exp(-i\nu\tau) d\nu \text{ and} \\ \tilde{E}_z(x, \tau) &= \int_{-\infty}^{\infty} \tilde{S}_z^{(v)}(x, \nu) \exp(-i\nu\tau) d\nu.\end{aligned}\quad (\text{B4})$$

By substituting (B4) into (B3) and using Jacobi-Anger expansion, $e^{\pm ip \sin \phi} = \sum_{n=-\infty}^{\infty} J_n(p) e^{\pm in\phi}$, where $J_n(p)$ is a Bessel function of the first kind of order k , we obtain the solution for the spectral amplitude $\hat{\rho}_{12}^{(v)}(x, \nu)$ in the form

$$\begin{aligned}\hat{\rho}_{12}^{(v)}(x, \nu) \\ = -i \frac{d_z n_{1r}^{(z)}}{2\hbar \gamma_z} \sum_{n=-\infty}^{\infty} J_n(P_{\Omega}^{(z)}) e^{i2n\Delta Kx} \frac{\tilde{S}_z^{(v)}(x, \nu + 2n\Omega)}{1 + i(\bar{\omega}_{1r}^{(z)} - \omega - \nu)/\gamma_z}.\end{aligned}\quad (\text{B5})$$

By combining Eqs. (B4) and (B5) for $\hat{\rho}_{12}(x, \tau)$, Eq. (B2) and the Jacobi-Anger expansion, one can write the solution for $\tilde{\rho}_{12}(x, \tau)$:

$$\begin{aligned}\tilde{\rho}_{12}(x, \tau) &= -i \frac{d_z n_{1r}^{(z)}}{2\hbar \gamma_z} \sum_{n,k=-\infty}^{\infty} J_n(P_{\Omega}^{(z)}) J_k(P_{\Omega}^{(z)}) e^{i2(n-k)\Delta Kx} \\ &\times \int_{-\infty}^{\infty} \frac{\tilde{S}_z^{(v)}(x, \nu + 2(n-k)\Omega)}{1 + i(\bar{\omega}_{1r}^{(z)} + 2k\Omega - \omega - \nu)/\gamma_z} e^{-i\nu\tau} d\nu.\end{aligned}\quad (\text{B6})$$

Putting this expression for $\tilde{\rho}_{12}(x, \tau)$ into the first equation of (B1) and using the spectral decomposition for $\tilde{E}_z(x, \tau)$, one obtains the following equation for $\tilde{S}_z^{(v)}(x, \nu)$:

$$\frac{\partial \tilde{S}_z^{(v)}(x, \nu)}{\partial x} = \sum_{k=-\infty}^{\infty} \frac{g_{\text{total}}^{(z)} J_k^2(P_{\Omega}^{(z)})}{1 + i(\tilde{\omega}_{tr}^{(z)} + 2k\Omega - \omega - \nu)/\gamma_z} \tilde{S}_z^{(v)}(x, \nu) + \sum_{\substack{n,k=-\infty \\ n \neq k}}^{\infty} \frac{g_{\text{total}}^{(z)} J_n(P_{\Omega}^{(z)}) J_k(P_{\Omega}^{(z)}) e^{i2(n-k)\Delta K x}}{1 + i(\tilde{\omega}_{tr}^{(z)} + 2k\Omega - \omega - \nu)/\gamma_z} \tilde{S}_z^{(v)}[x, \nu + 2(n-k)\Omega], \quad (\text{B7})$$

where $g_{\text{total}}^{(z)} = \frac{2\pi\omega N_{\text{ion}} n_{tr}^{(z)} d_z^2}{\hbar c \gamma_z \sqrt{\epsilon_{pl}^{(XUV)}}$ is the gain coefficient of z -polarized radiation in the absence of modulation. Assuming that the plasma has a strong dispersion at the frequency of the IR field, $g_{\text{total}}^{(z)}/\Delta K \ll 1$, one can neglect the second term in (B7) (see [31]). Thus, the solution for $\tilde{E}_z(x, \tau)$ takes the form

$$\tilde{E}_z(x, \tau) = \int_{-\infty}^{\infty} \tilde{S}_z^{(v)}(x=0, \nu) \exp \left[\sum_{k=-\infty}^{\infty} \frac{g_{\text{total}}^{(z)} J_k^2(P_{\Omega}^{(z)})}{1 + i(\tilde{\omega}_{tr}^{(z)} + 2k\Omega - \omega - \nu)/\gamma_z} \right] e^{-i\nu\tau} d\nu, \quad (\text{B8})$$

where $\tilde{S}_z^{(v)}(x=0, \nu)$ is the spectrum of z -polarization component of the XUV radiation at the entrance to the medium. For monochromatic incident XUV field (5) $\tilde{S}_z^{(v)}(x=0, \nu) = E_0^{(z)} \delta(\nu)$, where $\delta(\nu)$ is the Dirac delta function, and (B8) is rewritten as

$$\tilde{E}_z(x, \tau) = E_0^{(z)} \exp \left[\sum_{k=-\infty}^{\infty} \frac{g_{\text{total}}^{(z)} J_k^2(P_{\Omega}^{(z)})}{1 + i(\tilde{\omega}_{tr}^{(z)} + 2k\Omega - \omega)/\gamma_z} \right]. \quad (\text{B9})$$

In real conditions the frequency of the IR field is much larger than the gain linewidth, $\Omega \gg \gamma_z$. In such a case the z -polarized XUV radiation is most efficiently amplified if its frequency coincides with the time-average frequency of the $|1\rangle \leftrightarrow |2\rangle$ transition or is tuned from it to an even multiple of the modulation frequency: $\omega = \tilde{\omega}_{tr}^{(z)} + 2k\Omega$, where k is an integer. Under this condition, the z -polarization component of the monochromatic XUV radiation has the form (6).

Similarly, in the linear approximation, the y component of the XUV radiation in the medium satisfies the equations

$$\begin{aligned} \frac{\partial \tilde{E}_y}{\partial x} &= 4\pi N_{\text{ion}} d_y \frac{\omega}{c \sqrt{\epsilon_{pl}^{(XUV)}}} (\tilde{\rho}_{13} + \tilde{\rho}_{14}), \\ \frac{\partial \tilde{\rho}_{13}}{\partial \tau} + \{i(\tilde{\omega}_{tr}^{(y)} - \omega) + i\Delta_{\Omega}^{(y)} \cos[2(\Omega\tau + \Delta Kx)] + \gamma_y\} \tilde{\rho}_{13} &= n_{tr}^{(y)} \frac{d_y \tilde{E}_y}{2\hbar}, \\ \frac{\partial \tilde{\rho}_{14}}{\partial \tau} + \{i(\tilde{\omega}_{tr}^{(y)} - \omega) + i\Delta_{\Omega}^{(y)} \cos[2(\Omega\tau + \Delta Kx)] + \gamma_y\} \tilde{\rho}_{14} &= n_{tr}^{(y)} \frac{d_y \tilde{E}_y}{2\hbar}, \end{aligned} \quad (\text{B10})$$

where $\gamma_y \equiv \gamma_{13} = \gamma_{14}$ and $n_{tr}^{(y)} = \tilde{\rho}_{11}(x, \tau) - \tilde{\rho}_{33}(x, \tau) = \tilde{\rho}_{11}(x, \tau) - \tilde{\rho}_{44}(x, \tau)$ is the population difference at the $|1\rangle \leftrightarrow |3\rangle$ and $|1\rangle \leftrightarrow |4\rangle$ transitions, which in the case under consideration is the same and equal to $n_{tr}^{(y)} = 1$. Similar to z -polarized radiation, the y -polarized component of the XUV field is amplified most efficiently if the

carrier frequency of the field coincides with the $|1\rangle \leftrightarrow |3\rangle, |4\rangle$ transition frequency or is tuned from it by an even multiple of the modulation frequency: $\omega = \tilde{\omega}_{tr}^{(y)} + 2k'\Omega$, where k' is an integer. In this case, the solution of Eqs. (B10) for the monochromatic XUV radiation (5) has the form (7).

-
- [1] F. Krausz and M. Ivanov, Attosecond physics, *Rev. Mod. Phys.* **81**, 163 (2009).
 [2] M. Wu, S. Chen, S. Camp, K. J. Schafer, and M. B. Gaarde, Theory of strong-field attosecond transient absorption, *J. Phys. B* **49**, 062003 (2016).
 [3] L. Young, K. Ueda, M. Gühr, P. H. Bucksbaum, M. Simon, S. Mukamel, N. Rohringer, K. C. Prince, C. Masciovecchio, M. Meyer *et al.*, Roadmap of ultrafast x-ray atomic and molecular physics, *J. Phys. B* **51**, 032003 (2018).
 [4] R. Schoenlein, T. Elsaesser, K. Holldack, Z. Huang, H. Kapteyn, M. Murnane, and M. Woerner, Recent advances in

- ultrafast x-ray sources, *Philos. Trans. R. Soc. A* **377**, 20180384 (2019).
 [5] K. S. Budil, P. Salières, A. L'Huillier, T. Ditmire, and M. D. Perry, Influence of ellipticity on harmonic generation, *Phys. Rev. A* **48**, R3437(R) (1993).
 [6] P. Dietrich, N. H. Burnett, M. Ivanov, and P. B. Corkum, High-harmonic generation and correlated two-electron multiphoton ionization with elliptically polarized light, *Phys. Rev. A* **50**, R3585 (1994).
 [7] P. B. Corkum, Plasma Perspective on Strong-Field Multiphoton Ionization, *Phys. Rev. Lett.* **71**, 1994 (1993).

- [8] V. V. Strelkov, A. A. Gonoskov, I. A. Gonoskov, and M. Yu. Ryabikin, Origin for Ellipticity of High-Order Harmonics Generated in Atomic Gases and the Sub-Laser-Cycle Evolution of Harmonic Polarization, *Phys. Rev. Lett.* **107**, 043902 (2011).
- [9] A. Ferré, C. Handschin, M. Dumergue, F. Burgy, A. Comby, D. Descamps, B. Fabre, G. A. Garcia, R. Généaux, L. Merceron *et al.*, A table-top ultrashort light source in the extreme ultraviolet for circular dichroism experiments, *Nat Photonics* **9**, 93 (2015).
- [10] B. Vodungbo, A. B. Sardinha, J. Gautier, G. Lambert, C. Valentin, M. Lozano, G. Iaquaniello, F. Delmotte, S. Sebban, J. Lüning, and P. Zeitoun, Polarization control of high order harmonics in the EUV photon energy range, *Opt. Express* **19**, 4346 (2011).
- [11] J. Schmidt, A. Guggenmos, M. Hofstetter, S. H. Chew, and U. Kleineberg, Generation of circularly polarized high harmonic radiation using a transmission multilayer quarter waveplate, *Opt. Express* **23**, 33564 (2015).
- [12] X. Zhou, R. Lock, N. Wagner, W. Li, H. C. Kapteyn, and M. M. Murnane, Elliptically Polarized High-Order Harmonic Emission from Molecules in Linearly Polarized Laser Fields, *Phys. Rev. Lett.* **102**, 073902 (2009).
- [13] E. Skantzakis, S. Chatziathanasiou, P. A. Carpeggiani, G. Sansone, A. Nayak, D. Gray, P. Tzallas, D. Charalambidis, E. Hertz, and O. Faucher, Polarization shaping of high-order harmonics in laser-aligned molecules, *Sci. Rep.* **6**, 39295 (2016).
- [14] G. Lambert, B. Vodungbo, J. Gautier, B. Mahieu, V. Malka, S. Sebban, P. Zeitoun, J. Luning, J. Perron, A. Andreev *et al.*, Towards enabling femtosecond helicity-dependent spectroscopy with high-harmonic sources, *Nat. Commun.* **6**, 6167 (2015).
- [15] C. Zhai, R. Shao, P. Lan, B. Wang, Y. Zhang, H. Yuan, S. M. Njoroge, L. He, and P. Lu, Ellipticity control of high-order harmonic generation with nearly orthogonal two-color laser fields, *Phys. Rev. A* **101**, 053407 (2020).
- [16] A. Fleischer, O. Kfir, T. Diskin, P. Sidorenko, and O. Cohen, Spin angular momentum and tunable polarization in high-harmonic generation, *Nat. Photonics* **8**, 543 (2014).
- [17] O. Kfir, P. Grychtol, E. Turgut, R. Knut, D. Zusin, D. Popmintchev, T. Popmintchev, H. Nembach, J. M. Shaw, A. Fleischer *et al.*, Generation of bright phase-matched circularly-polarized extreme ultraviolet high harmonics, *Nat. Photonics* **9**, 99 (2015).
- [18] T. Fan, P. Grychtol, R. Knut, C. Hernández-Garsía, D. D. Hickstein, D. Zusin, C. Gentry, F. J. Dollar, C. A. Mancuso, C. W. Hogle *et al.*, Bright circularly polarized soft x-ray high harmonics for x-ray magnetic circular dichroism, *Proc. Nat. Acad. Sci. USA* **112**, 14206 (2015).
- [19] K. C. Westfold, The polarization of synchrotron radiation, *Astrophys. J.* **130**, 241 (1959).
- [20] U. Heinzmann, Experimental determination of the phase differences of continuum wavefunctions describing the photoionisation process of xenon atoms. I. Measurements of the spin polarisations of photoelectrons and their comparison with theoretical results, *J. Phys. B: Atom. Mol. Phys.* **13**, 4353 (1980).
- [21] G. Schütz, W. Wagner, W. Wilhelm, P. Kienle, R. Zeller, R. Frahm, and G. Materlik, Absorption of Circularly Polarized X Rays in Iron, *Phys. Rev. Lett.* **58**, 737 (1987).
- [22] C. T. Chen, F. Sette, Y. Ma, and S. Modesti, Soft-x-ray magnetic circular dichroism at the $L_{2,3}$ edges of nickel, *Phys. Rev. B* **42**, 7262 (1990).
- [23] V. Schmidt, Photoionization of atoms using synchrotron radiation, *Rep. Prog. Phys.* **55**, 1483 (1992).
- [24] N. Böwering, T. Lischke, B. Schmidtke, N. Müller, T. Khalil, and U. Heinzmann, Asymmetry in Photoelectron Emission from Chiral Molecules Induced by Circularly Polarized Light, *Phys. Rev. Lett.* **86**, 1187 (2001).
- [25] S. Sasaki, Analyses for a planar variably-polarizing undulator, *Nucl. Instrum. Methods Phys. Res. A* **347**, 83 (1994).
- [26] E. Allaria, D. Castronovo, P. Cinquegrana *et al.*, Two-stage seeded soft-x-ray free-electron laser, *Nat. Photonics* **7**, 913 (2013).
- [27] E. A. Schneidmiller and M. V. Yurkov, Obtaining high degree of circular polarization at x-ray free electron lasers via a reverse undulator taper, *Phys. Rev. ST Accel. Beams* **16**, 110702 (2013).
- [28] E. Ferrari, E. Allaria, J. Buck, G. De Ninno, B. Diviacco, D. Gauthier, L. Giannessi, L. Glaser, Z. Huang, M. Ilchen *et al.*, Single shot polarization characterization of XUV FEL pulses from crossed polarized undulators, *Sci. Rep.* **5**, 13531 (2015).
- [29] A. A. Lutman, J. P. MacArthur, M. Ilchen *et al.*, Polarization control in an x-ray free-electron laser, *Nat. Photonics* **10**, 468 (2016).
- [30] A. Depresseux, E. Oliva, J. Gautier, F. Tissandier, G. Lambert, B. Vodungbo, J.-P. Goddet, A. Tafzi, J. Nejdil, M. Kozlova *et al.*, Demonstration of a Circularly Polarized Plasma-Based Soft-X-Ray Laser, *Phys. Rev. Lett.* **115**, 083901 (2015).
- [31] V. A. Antonov, K. Ch. Han, T. R. Akhmedzhanov, M. Scully, and O. Kocharovskaya, Attosecond Pulse Amplification in a Plasma-Based X-Ray Laser Dressed by an Infrared Laser Field, *Phys. Rev. Lett.* **123**, 243903 (2019).
- [32] I. R. Khairulin, V. A. Antonov, M. Yu. Ryabikin, M. A. Berrill, V. N. Shlyaptsev, J. J. Rocca, and Olga Kocharovskaya, Amplification of elliptically polarized sub-femtosecond pulses in neon-like x-ray laser modulated by an IR field, *Sci. Rep.* **12**, 6204 (2022).
- [33] T. Boehly, M. Rusotto, R. S. Craxton, R. Epstein, B. Yaakobi, L. B. Da Silva, J. Nilsen, E. A. Chandler, D. J. Fields, B. J. Mac Gowan *et al.*, Demonstration of a narrow-divergence x-ray laser in neon-like titanium, *Phys. Rev. A* **42**, 6962(R) (1990).
- [34] P. V. Nickles, V. N. Shlyaptsev, M. Kalachnikov, M. Schnürer, I. Will, and W. Sandner, Short Pulse X-Ray Laser at 32.6 Nm Based on Transient Gain in Ne-like Titanium, *Phys. Rev. Lett.* **78**, 2748 (1997).
- [35] J. Nilsen, Y. Li, and J. Dunn, Modeling picosecond-laser-driven neonlike titanium x-ray laser experiments, *J. Opt. Soc. Am. B* **17**, 1084 (2000).
- [36] D. Alessi, B. M. Luther, Y. Wang, M. A. Larotonda, M. Berrill, and J. J. Rocca, High repetition rate operation of saturated table-top soft x-ray lasers in transitions of neon-like ions near 30 nm, *Opt. Express* **13**, 2093 (2005).
- [37] J. J. Rocca, Table-top soft x-ray lasers, *Rev. Sci. Instrum.* **70**, 3799 (1999).
- [38] O. Guilbaud, S. Kazamias, K. Cassou, O. Delmas, J. Demailly, O. Neveu, D. Ros, E. Baynard, M. Pittman, M. Shazad *et al.*, Seeded operation of a Ne-like titanium soft x-ray laser, in *X-Ray Lasers, Springer Proceedings in Physics*, edited by J. Rocca,

- C. Menoni, and M. Marconi (Springer, Cham, 2016), Vol. 169, pp. 61–67.
- [39] J. J. Rocca, F. G. Tomasel, M. C. Marconi, V. N. Shlyaptsev, J. L. A. Chilla, B. T. Szapiro, and G. Giudice, Discharge-pumped soft-x-ray laser in neon-like argon, *Phys. Plasmas* **2**, 2547 (1995).
- [40] Y. Li, G. Pretzler, and E. E. Fill, Ne-like ion lasers in the extreme ultraviolet region, *Phys. Rev. A* **52**, R3433(R) (1995).
- [41] J. C. Moreno, R. C. Cauble, P. M. Celliers, L. B. Da Silva, J. Nilsen, and A. S. Wan, Development of a short-pulse Ne-like x-ray laser, in *Soft X-Ray Lasers and Applications Proceedings of the SPIE*, edited by J. J. Rocca and P. L. Hagelstein (SPIE, Philadelphia, 1995), Vol. 2520, p. 97.
- [42] Y. Zhang, J. Zhang, S.-B. Liu, D.-Z. Zhang, and Y.-X. Nie, Transient Ne-like Cr x-ray lasers driven by picosecond laser pulses, *Phys. Plasmas* **5**, 266 (1998).
- [43] L. Urbanski, M. C. Marconi, L. M. Meng, M. Berrill, O. Guilbaud, A. Klisnick, and J. J. Rocca, Spectral linewidth of a Ne-like Ar capillary discharge soft-x-ray laser and its dependence on amplification beyond gain saturation, *Phys. Rev. A* **85**, 033837 (2012).
- [44] H. Daido, Review of soft x-ray laser researches and developments, *Rep. Prog. Phys.* **65**, 1513 (2002).
- [45] S. Suckewer and P. Jaeglé, X-ray laser: Past, present, and future, *Laser Phys. Lett.* **6**, 411 (2009).
- [46] M. Berrill, Y. Wang, M. A. Larotonda, B. M. Luther, V. N. Shlyaptsev, and J. J. Rocca, Pump pulse-width dependence of grazing-incidence pumped transient collisional soft-x-ray lasers, *Phys. Rev. A* **75**, 063821 (2007).
- [47] M. Chini, B. Zhao, H. Wang, Y. Cheng, S. X. Hu, and Z. Chang, Subcycle Ac Stark Shift of Helium Excited States Probed with Isolated Attosecond Pulses, *Phys. Rev. Lett.* **109**, 073601 (2012).
- [48] M. F. Gu, The flexible atomic code, *Can. J. Phys.* **86**, 675 (2008).
- [49] I. R. Khairulin, V. A. Antonov, M. Yu. Ryabikin, and O. Kocharovskaya, Sub-fs pulse formation in a seeded hydrogenlike plasma-based x-ray laser dressed by an infrared field: Analytical theory and numerical optimization, *Phys. Rev. Res.* **2**, 023255 (2020).
- [50] V. S. Popov, Tunnel and multiphoton ionization of atoms and ions in a strong laser field (Keldysh theory), *Phys. Usp.* **47**, 855 (2004).
- [51] D. Woodbury, L. Feder, V. Shumakova, C. Gollner, R. Schwartz, B. Miao, F. Salehi, A. Korolov, A. Pugžlys, A. Baltuška, and H. M. Milchberg, Laser wakefield acceleration with mid-IR laser pulses, *Opt. Lett.* **43**, 1131 (2018).
- [52] Z. Samsonova, S. Höfer, V. Kaymak, S. Ališauskas, V. Shumakova, A. Pugžlys, A. Baltuška, T. Siefke, S. Kroker, A. Pukhov *et al.*, Relativistic Interaction of Long-Wavelength Ultrashort Laser Pulses with Nanowires, *Phys. Rev. X* **9**, 021029 (2019).
- [53] A. G. Ciriolo, M. Negro, M. Devetta, E. Cinquanta, D. Faccialà, A. Pusala, S. De Silvestri, S. Stagira, and C. Vozzi, Optical parametric amplification techniques for the generation of high-energy few-optical-cycles IR pulses for strong field applications, *Appl. Sci.* **7**, 265 (2017).
- [54] A. Dubietis and A. Matijošius, Table-top optical parametric chirped pulse amplifiers: Past and present, *Opto-Electron. Adv.* **6**, 220046 (2023).
- [55] M. Born and E. Wolf, *Principles of Optics* (Pergamon Press, New York, 1964).
- [56] S. Guérin, P. Mora, J. C. Adam, A. Héron, and G. Laval, Propagation of ultraintense laser pulses through overdense plasma layers, *Phys. Plasmas* **3**, 2693 (1996).
- [57] G. Li, R. Yan, C. Ren, T.-L. Wang, J. Tonge, and W. B. Mori, Laser Channeling in Millimeter-Scale Underdense Plasmas of Fast-Ignition Targets, *Phys. Rev. Lett.* **100**, 125002 (2008).
- [58] A. Depresseux, E. Oliva, J. Gautier, F. Tissandier, J. Nejdil, M. Kozlova, G. Maynard, J. P. Goddet, A. Tafzi, A. Lifschitz *et al.*, Table-top femtosecond soft x-ray laser by collisional ionization gating, *Nat. Photonics* **9**, 817 (2015).
- [59] A. K. Pandey, I. Papagiannouli, F. Sanson, E. Baynard, J. Demailly, S. Kazamias, M. Pittman, O. Neveu, B. Lucas, A. Le Marec *et al.*, Towards subpicosecond pulses from solid target plasma based seeded soft x-ray laser, *Opt. Express* **28**, 28924 (2020).
- [60] L. D. Landau and E. M. Lifshitz, *Quantum Mechanics: Non-relativistic Theory*, 3rd ed. (Pergamon Press Inc., New York, 1977), pp. 82–101.
- [61] I. I. Sobelman, *Atomic Spectra and Radiative Transitions*, Springer Series on Atoms + Plasmas Book Series, Vol. 12 (Springer-Verlag, Berlin, Heidelberg, 1992), pp. 200–302.
- [62] V. A. Antonov, Y. V. Radeonychev, and O. Kocharovskaya, Formation of ultrashort pulses via quantum interference between Stark-split atomic transitions in a hydrogenlike medium, *Phys. Rev. A* **88**, 053849 (2013).
- [63] M. Gross and S. Haroche, Superradiance: An essay on the theory of collective spontaneous emission, *Phys. Rep.* **93**, 301 (1982).